Materials Advances

ROYAL SOCIETY OF CHEMISTRY

REVIEW

View Article Online
View Journal

Cite this: DOI: 10.1039/d6ma00039h

Carbon quantum dot-based thin films for multifunctional and sustainable applications

Arup Kumer Roy, [a] Ayesha Binth Humayun, [b] Yuv-raj Acharjee, [a] Nusrat Jahan Usha [b] and Sumit Majumder *[b]

Carbon quantum dots (CQDs) have attracted significant attention as a versatile class of nanomaterials owing to their abundance, biocompatibility, and highly tunable functional properties. Their optical, electronic, and chemical characteristics are strongly governed by particle size, surface functional groups, and heteroatom doping, while their carbon-based composition makes them attractive candidates for low-toxicity and biocompatible systems. CQDs are typically integrated into solid matrices, particularly polymer-based thin films, not only to suppress nanoparticle aggregation and environmental degradation but also to realize functional applications. Such integration also enhances the stability, reliability, and reproducibility of CQD-based composites, enabling their use for applications ranging from bioimaging and wearable sensing to antimicrobial and antifouling coatings, environmental remediation, and flexible optoelectronic devices. However, precise control over CQD size, surface chemistry, and dispersion within solid matrices, as well as scalable and reproducible fabrication of CQD-based films compatible with industrial processing, remains challenging. Moreover, ensuring long-term structural, optical, and functional stability of CQD-based films under practical operating conditions is essential for their reliable and widespread deployment. This review provides a comprehensive overview of recent progress in CQD-based films, with emphasis on CQD synthesis and film fabrication strategies, key application areas, associated challenges, and future research directions.

Received 7th January 2026,
Accepted 26th March 2026

DOI: 10.1039/d6ma00039h

rsc.li/materials-advances

1 Introduction

Carbon quantum dots (CQDs) are zero-dimensional nanomaterials with characteristic sizes below 10 nanometers.[1] CQDs typically exhibit a core–shell structure dominated by crystalline sp^2-carbon domains, although amorphous regions containing sp^2 and sp^3 carbons can also be present.[2] The sp^2-rich domains act as quantum-confined regions with discrete energy levels, thereby giving rise to stable photoluminescence (PL). Additionally, CQDs exhibit strong absorption in the ultraviolet (UV) region, which arises from π–π* transitions of C=C bonds and n–π* transitions associated with C=O groups.[3]

CQDs possess surface defects and abundant functional groups, including hydroxyl (–OH), carboxyl (–COOH), carbonyl (–C=O), amine ($–NH_2$), and thiol (–SH) groups.[4] Depending on the precursor and synthesis conditions, heteroatoms such as nitrogen (N), boron (B), phosphorus (P), and sulfur (S) may also be incorporated into their structure.[5] The size, surface chemistry and heteroatom doping strongly influence the optical, electronic, and chemical properties of CQDs (Fig. 1).[6] Additionally, their carbon-based composition contributes to realizing non-toxic, bio-compatible nanomaterials,[7] making them promising candidates for diverse applications including bioimaging, wearable sensors, antimicrobial and antifouling coatings, environmental remediation, and flexible optoelectronic devices.

CQDs are synthesized *via* top-down methods in which bulk carbon materials, such as graphite or carbon soot, are broken down into nanoscale fragments.[1,6,7] In contrast, bottom-up approaches employ biomass-derived or synthetic molecular precursors to synthesize CQDs.[1,6,7] The latter methods offer superior control over particle size, surface functional groups, and heteroatom doping, thereby enabling precise tuning of CQD properties including their surface chemistry, catalytic behaviour, PL, and solubility.

However, for practical applications, CQDs are typically incorporated into solid polymer matrices,[8] such as polyvinyl alcohol (PVA), cellulose, or polyvinylidene fluoride (PVDF), enabling controlled modification of the composite's optical, electronic, and chemical properties. Furthermore, integration into thin polymer films suppresses nanoparticle aggregation, enhances photostability and environmental stability, and enables direct integration into devices with controlled CQD

[a] Department of Chemistry, Chittagong University of Engineering and Technology, Chattogram-4349, Bangladesh
[b] Department of Biomedical Engineering, Chittagong University of Engineering and Technology, Chattogram-4349, Bangladesh. E-mail: s.majumder@cuet.ac.bd

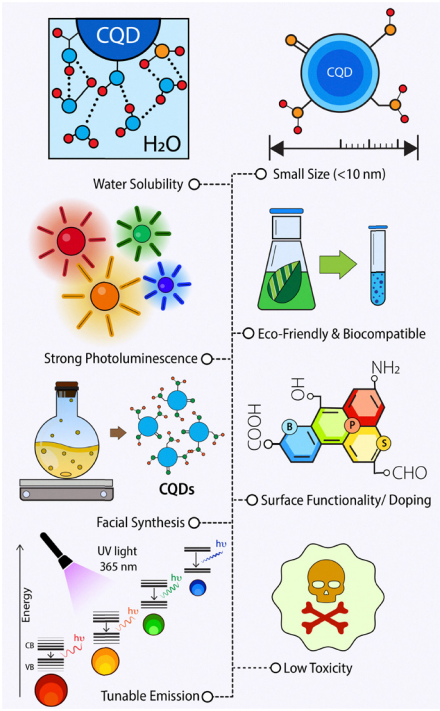

Fig. 1 Properties of carbon quantum dots (CQDs).

distribution. These properties render CQD-based films a versatile platform for biomedical, environmental, smart food packaging, and anti-counterfeiting applications (Fig. 2).[9,10]

Nevertheless, several challenges continue to limit the large-scale application of CQD-based films. A major concern arises from the variability in the size, composition, and surface chemistry of CQDs, which stems from limited control and reproducibility during synthesis.[11,12] Additionally, achieving uniform dispersion over large areas and scaling consistent film fabrication remain significant engineering challenges. Furthermore, some CQDs have been reported to pose ecological risks, raising important safety and environmental concerns.[13–16] Addressing these interrelated challenges is essential for the reproducible, sustainable fabrication and broader adoption of CQD-based films.

In this paper, we review recent advancements in CQD-based thin films, highlighting the influence of CQD precursors and synthesis, material properties, and fabrication techniques on film morphology and device performance, while outlining key challenges for their widespread adoption. Section 2 covers CQD synthesis and functionalization alongside film fabrication methods, while major film classes and their optical, electronic, catalytic, and antimicrobial characteristics are discussed in Section 3. Progress in film fabrication techniques and integration approaches across diverse application settings is presented in Section 4. Section 5 addresses key challenges and concerns, including synthesis reproducibility, large-scale manufacturing, and environmental safety. Finally, this paper concludes in Section 6 by outlining future perspectives on the potential of CQD-based films in advancing next-generation material technologies.

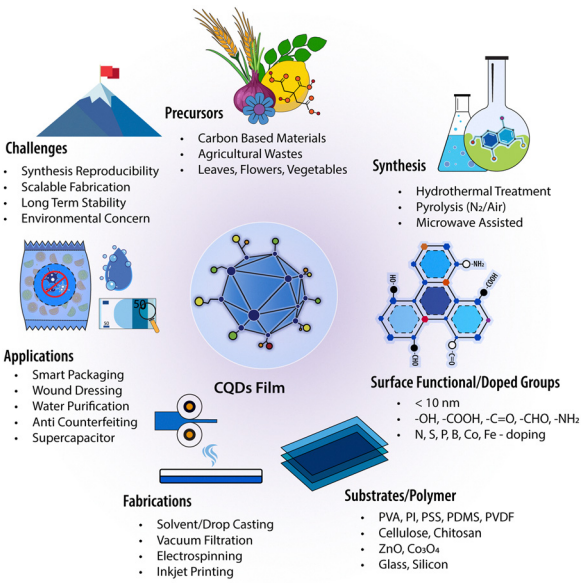

Fig. 2 CQD-based thin films – synthesis, fabrication, applications and challenges.

2 Carbon quantum dot synthesis

2.1 Precursors for CQD synthesis

2.1.1 Green precursors. Carbon quantum dots (CQDs) can be synthesized from a wide range of biomass resources, including household food waste, agricultural residues, leaves, seeds, flowers, and fruits, making them a sustainable, environmentally friendly, and cost-effective class of nanomaterials. Household food residues, particularly fruit and vegetable peels, have been widely reported as effective precursors for CQD synthesis.[17–27] Hard biomass materials such as nut and fruit shells,[28–32] as well as crustacean wastes,[33–35] have also been widely utilized. Additionally, agricultural by-products,[36–46] plant leaves,[47–63] and seeds[64–73] serve as abundant and low-cost carbon sources for CQD synthesis. These biodegradable materials typically contain high concentrations of carbohydrates, proteins, amino acids, polyphenols, and naturally occurring heteroatoms, which facilitate efficient carbonization and can enable *in situ* nitrogen or sulfur doping during CQD formation.

Alliums, such as garlic,[74] and onion[75] contain organosulfur compounds that act as intrinsic sulfur heteroatom dopants during carbonization, thereby enhancing the PL and electrochemical performance of the resulting CQDs. Floral waste, including various flower petals,[76–86] as well as cotton,[87] has also been reported to yield highly fluorescent, stable, and water-dispersible functionalized CQDs suitable for imaging, sensing, photocatalysis, and environmental remediation applications. Similarly, fruits[88–95] and their processed derivatives, such as fruit juices and pomace,[95–99] have been widely investigated as CQD precursors. These sources provide natural sugars, amino

Table 1 CQD precursors and heteroatom-doped CQDs

Category	Biomass precursors/compounds	Dopants	Key features
Fruit and vegetable peels	Dragon fruit,[17] lemon,[18] orange,[20] pomegranate,[21,22] banana,[23,24] pomelo,[25] water melon,[26] garlic,[27] onion[19]	N, S	• High carbohydrate content enabling carbonization • Organic acids/polyphenols assist surface passivation • Introduces oxygen-containing surface groups
Nut and fruit shells	Walnut,[28,29] peanut,[30] pistachio,[31] and durian[32]	N, S	• Lignocellulosic carbon-rich biomass • Aromatic frameworks promote graphitic domains
Crustacean waste	Prawn,[33] shrimp,[34] and crab shells[35]	N, S	• Chitin-rich biomolecules enable N doping
Agricultural byproducts	Onion waste,[36] barley bran,[37] rice husks,[39] coconut husks,[40] sugarcane wastes and molasses,[41,42] wheat bran,[43] wheat straw,[44] lignin,[45,46] and willow bark[38]	N, S, B	• Abundant lignocellulosic biomass • Aromatic C structures favor graphitic CQDs • Natural heteroatoms support *in situ* doping
Leaves	Artichoke,[47] bamboo,[48] celery,[56] coriander,[57] cauliflower leaves,[58] ginkgo,[59] hemp,[60] laurel,[61] mango,[62] maple,[63] neem,[49] peach,[50] purslane,[51] tea,[52] teak,[53] tobacco,[54] and tulsi[55]	N	• N-rich biomolecules and polyphenols • Supports heteroatom incorporation and surface functionalization
Seeds and grains	Castor,[64] finger millet,[65] kidney beans,[66] fennel,[67] chia,[68] watermelon,[69] fenugreek,[70] carom,[71] lychee,[72] and dates[73]	N	• Rich in proteins, lipids, and carbohydrates • Provides nitrogenous biomolecules for tunable surface chemistry
Alliums	Garlic[74] and onion[75]	S	• Organosulfur compounds enable intrinsic S doping • Improves PL and electrochemical activity
Floral waste	Rose,[76,77] roselle,[79] magnolia,[80] mahua (*M. longifolia*),[81] marigold,[82,83] chinese plum (*P. mume*),[84] *R. hispida*,[85] chestnut rose (*R. roxburghii*),[86] cotton,[87] and crown flower (*C. gigantea*)[78]	N, S	• Flavonoids/pigments/polyphenols promote strong photoluminescence • Enables stable, water-dispersible CQD formation
Fruits and derivatives	Apple,[88] cherry tomatoes,[89] guava,[90] lemon,[91] orange pomace,[92] palm,[93] unripe peach,[94] and watermelon[95] **Derivatives**: apple,[96] orange,[97] mulberry,[98] and watermelon juices[95,99]	N, S	• Sugars and organic acids support carbonization • Amino acids and polyphenols aid surface passivation
Nitrogen sources	**Organic**: biomass,[108] chitosan,[110] and gelatin[111] **Amines**: phenylenediamine,[109] EDA,[112] *o*-PD,[113] 1,4-butanediamine,[114] EA,[115] PEI,[116] urea,[117] thiourea,[118] DETA,[119] and $NH_3{\cdot}H_2O$[120] **Amino acids**: glycine,[121] L-arginine,[122] and L-lysine,[123] L-Glutamine[124] and L-cysteine[125]	N	• Provides abundant amine groups • Enables controlled N-doping (pyridinic, pyrrolic, and graphitic N) • Enhances fluorescence efficiency and surface reactivity
Chalcogen sources	Thiomalic acid,[126] thioglycolic acid,[127] thioacetic acid,[128] SDS,[131] sodium thiosulfate,[132] and thiourea[129] Sulfisoxazole + PMSO + $PMSO_2$[130]	S	• Supplies –SH/–SO/–SO_2 groups for lattice or surface doping • Modulates CQD band structure and PL
	Selenocystine,[134] sodium selenite[135,136] L-Selenocysteine[137,138] and algae biomass[139]	Se	• Se enhances ROS generation and solubility
Boron sources	BBr_3,[141] boric acid,[142,143] and phenylboronic acid[144]	B	• Incorporates B with minimal C lattice distortion • Enhances optical properties
Cobalt sources	Cobalt acetate[145] and hexamine cobalt chloride[146]	Co	• Co introduces catalytic and sensing functionality
Silver sources	Silver nitrate ($AgNO_3$)[181]	Ag	• Enhances antibacterial activity[182] • Increases electron transfer ability
Halogen sources	**F**: 4,5-Difluorobenzene-1,2-diamine,[151] tetrafluoroterephthalic acid,[152] and 2,2,3,3,4,4-hexafluoro-1,5-pentanediol diglycidyl ether[153]	F, Cl, Br, I	• Strongly electronegative dopants alter CQD electronic structure
	Cl: HCl,[154] sucralose,[155] and thionyl chloride[156]		• Electron-withdrawing effects shift energy levels, introduce surface states and modify PL emission
	Br: 3-Bromo-1,2-phenylenediamine[154] and HBr[157,158]		• Tunes optical absorption and surface polarity.
	I: Iodobenzoic acid[159] and KI[160]		

BBr_3: boron tribromide, DETA: diethylenetriamine, EA: ethanolamine, EDA: ethylenediamine, HBr: hydrobromic acid, HCl: hydrochloric acid, KI: potassium iodide, $NH_3{\cdot}H_2O$: aqueous ammonia, *o*-PD: *ortho*-phenylenediamine, PEI: polyethylenimine, PMSO: methyl phenyl sulfoxide, $PMSO_2$: methyl phenyl sulfone, SDS: sodium dodecyl sulfate.

acids, cellulose, organic acids, and polyphenols that promote efficient carbonization and surface passivation during CQD formation.[100] A comprehensive list of representative green precursors used for CQD synthesis is presented in Table 1.

2.1.2 Heteroatom doping. The electronic structure of CQDs can be tailored through heteroatom doping, which alters charge distribution, introduces defect states, and modifies surface functional groups (Fig. 3). These structural changes directly influence the PL, optical behavior, and catalytic activity.[101–103] In general, highly electronegative dopants such as nitrogen (N) or sulfur (S) can result in surface passivation,[104] enhanced fluorescence quantum yield (QY),[104] and blue-shifted emission in certain CQD systems,[105] whereas dopants with lower electronegativity, including phosphorus (P), boron (B), or selenium (Se), may introduce mid-gap or defect states that shift the emission toward longer wavelengths.[106] These effects of doping allow for controlled modulation of the optical band structure and emission wavelength of CQDs.

Nitrogen is one of the most extensively investigated dopants in CQDs, as it introduces electron-rich active sites that enhance fluorescence efficiency and modify the surface chemistry of N-doped CQDs (N-CQDs). Nitrogen-doped CQDs typically exhibit pyridinic N, pyrrolic N, and graphitic N configurations,[107] along with surface functional groups such as oxidized nitrogen species (N-oxides), amines ($-NH_2$), and oxygen-containing groups (–COOH and –OH).[9] These functional groups contribute to their high water solubility and fluorescence properties. N-CQDs are commonly synthesized using nitrogen-containing natural biomass precursors.[108] Additionally, nitrogen-rich organic molecules,[109–111] including amine-based compounds[112–120] and amino acids,[121–125] have been used as effective precursors for the controlled synthesis of N-CQDs.

Another widely studied class of heteroatoms investigated for CQD doping include chalcogens such as sulfur (S) and selenium (Se). Sulfur doping is typically achieved using a variety of S-containing precursors such as organosulfur compounds,[74,75,126–130] surfactants,[131] and inorganic salts.[132] These precursors provide reactive functional groups including –SH, –SO, $-SO_2$, and thioether (R–S–R′), which facilitate the incorporation of sulfur into the carbon framework during CQD formation. However, the comparable electronegativities of carbon and sulfur often limit charge transfer within the doped CQD structure, thereby influencing the optical, electronic, and catalytic properties of the resulting CQDs.[133] Additionally, Se-doped CQDs (Se-CQDs) are synthesized from Se-based precursors,[134–139] including amino acids such as selenocystine[134] and L-selenocysteine,[137,138] as well as algae biomass.[139] Se-CQDs are known for their biocompatibility, high water solubility, favorable optical properties, and enhanced reactive oxygen species (ROS) production capability.[134,140]

Other single-heteroatom-doped CQDs, including boron-doped (B-CQDs)[141–144] and cobalt-doped CQDs (Co-CQDs),[145,146] have also been reported to show enhanced catalytic and electrochemical performance in CQD-based materials.[147] Boron is particularly effective due to its comparable atomic size to carbon, which allows for its efficient incorporation into the carbon lattice with minimal strain, thus enhancing the optical and catalytic performance of CQDs.[148]

Halogen-doped CQDs have attracted significant attention because the strong electronegativity of halogen atoms enables effective modulation of the electronic and optical properties of CQDs.[149] For example, fluorine-doped CQDs (F-CQDs) exhibit strong electron-withdrawing effects due to the high electronegativity of fluorine (χ = 3.98), which can modify the electronic structure and introduce new surface states, thereby inducing red-shifted photoluminescence in certain CQD systems.[150] Various halogen-containing precursors have been employed to synthesize F-,[151–153] Cl-,[154–156] Br-,[154,157,158] and I-doped CQDs,[159,160] as summarized in Table 1.

Some studies have used multiple precursors to co-dope CQDs with different heteroatoms in order to enhance their optical, electronic, and chemical properties through synergistic interactions between the dopants and the carbon framework.[6] For example, boron and nitrogen co-doped CQDs (B,N-CQDs) have been synthesized using boron sources such as boric acid,[161,162] sodium borohydride,[163] and 3-carboxyphenylboronic acid,[164] in combination with nitrogen-rich precursors like EDA, dopamine, and L-DOPA. Similarly, sulfur and nitrogen co-doped CQDs (S,N-CQDs) have been produced from various sulfur-based precursors, including thiosemicarbazide,[165,166] thiourea,[167] L-cysteine,[168,169] thionin,[170] and sodium sulfide,[171,172] along with nitrogen sources including chitosan, glutamine, and PEI. Furthermore, sulfur and selenium co-doped CQDs (S,Se-CQDs) have been reported for applications in biological imaging and ROS scavenging,[173] typically utilizing citric acid, mercaptoethylamine, and sodium selenite as the carbon, sulfur, and selenium sources, respectively.

Priyadharshini *et al.* synthesized CQDs co-doped with three heteroatoms (N, Zn, and B) using tartaric acid, zinc chloride,

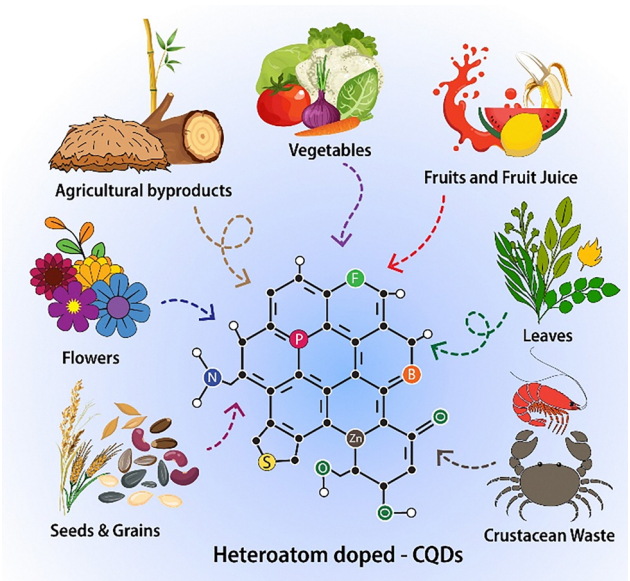

Fig. 3 Precursors for CQD synthesis and heteroatom doping.

and pyrimidine-5-boronic acid as the respective precursors.[174] The resulting CQDs exhibited high fluorescence sensitivity toward Co^{2+} ions in water. In another study, Co, N, and S co-doped CQDs were produced from citric acid, methionine, and cobalt acetate as the respective C, C/N/S, and Co sources, respectively, for fluorescence-based detection of pregabalin in pharmaceutical capsules.[145]

2.2 Synthesis methods

In the literature, a variety of methods have been explored for the efficient synthesis of CQDs, which are broadly classified into top-down and bottom-up methods.[175] The selection of a synthesis method generally depends on the desired properties of the CQDs, including size and morphology, PL efficiency, and surface chemistry,[4,135] as well as the nature of the precursor materials used.[176]

In top-down processes, carbon-rich materials such as bulk carbon,[9,177] graphite,[178] and carbon nanotubes[179] are broken down into nanoscale particles using physical or chemical methods, including arc discharge, ball milling, laser ablation, chemical or electrochemical oxidation, and ultrasonication.[180]

Although these techniques are relatively straightforward and suitable for producing CQDs from diverse precursor materials, they generally offer limited control over particle size, morphology, and surface functionalization, which can influence subsequent CQD–polymer interactions, film uniformity and device performance.[9] Additionally, top-down approaches require long processing times and harsh conditions, such as high temperatures, elevated pressures, or strong oxidizing agents, to effectively decompose the carbon matrix.[183]

In contrast, bottom-up methods synthesize CQDs from small organic molecules or biomass-derived precursors through carbonization, polymerization, and thermal decomposition (Fig. 4).

Common bottom-up techniques include hydrothermal or solvothermal treatment, microwave-assisted synthesis, and thermal pyrolysis.[184] In these processes, molecular precursors such as carbohydrates, organic acids, amines, amino acids, and polymeric materials undergo sequential dehydration, polymerization, and carbonization, resulting in nanoscale carbon particles with abundant surface functional groups and enhanced control over particle size, morphology, and physicochemical properties that promote effective dispersion, strong polymer interactions, and uniform, high-performance CQD-based films.[107]

The crude product obtained after CQD synthesis often contains unreacted precursors, small molecular fluorophores, inorganic salts, and amorphous carbon particles.[185] These impurities can significantly influence their optical response, surface chemistry, and reproducibility. Therefore, appropriate purification strategies are required to isolate well-defined CQDs with stable physicochemical characteristics. Common purification techniques include dialysis, centrifugation, solvent extraction, electrophoresis, and column chromatography.[186] In practice, centrifugation is often used to remove large carbonaceous aggregates, whereas dialysis uses semipermeable membranes to eliminate small molecular impurities and inorganic salts. Additionally, chromatographic methods provide versatile and highly efficient approaches for high-resolution separation of CQDs based not only on size but also on surface chemistry or polarity. Such purified CQDs exhibit improved dispersion and interfacial interactions within polymer matrices, thereby enhancing the optical and electronic performance of CQD-based thin films.[186,187]

A more extensive discussion of CQD synthesis methodologies is available in several studies.[175,180,183,188]

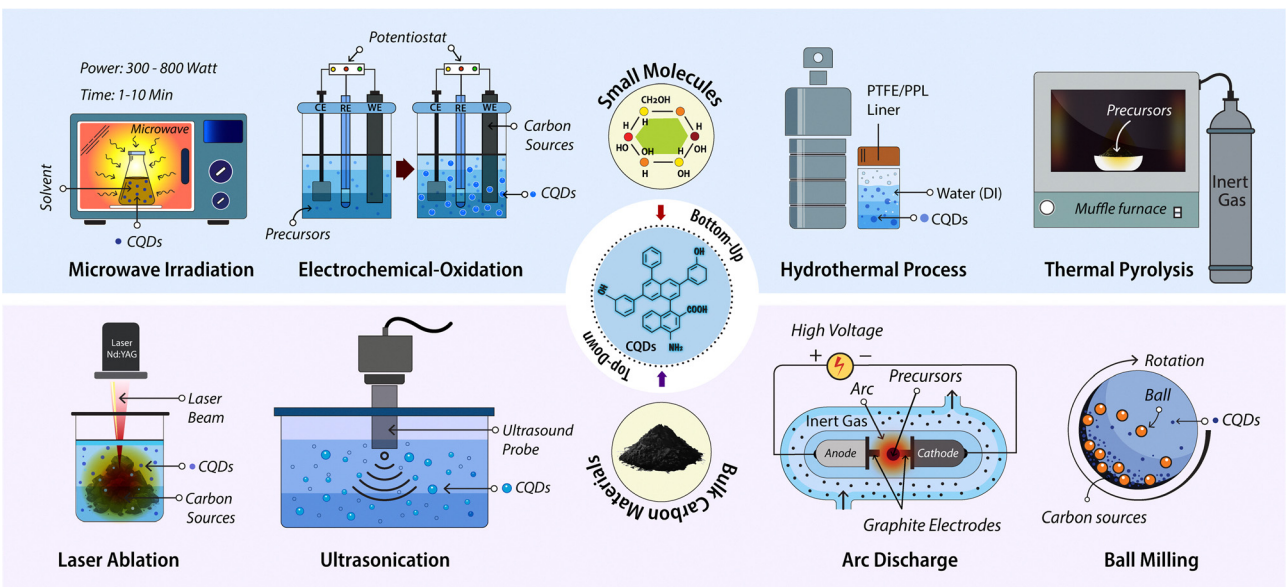

Fig. 4 Carbon quantum dot synthesis methods.

3 Fabrication of CQD-based films

Researchers have been exploring facile and cost-effective techniques for incorporating functionalized CQDs into polymer matrices to enable scalable production of thin films. Polymers such as PVA, PVDF, PPy, chitosan and cellulose are frequently reported for their excellent film-forming capabilities. The hydroxyl (–OH) groups of PVA, chitosan, and cellulose (including derivatives such as carboxymethyl cellulose and cellulose acetate) interact with the surface functional groups of CQDs, such as hydroxyl (–OH), carboxyl (–COOH), and carbonyl (C═O), as well as amine groups (–NH_2, when present), primarily through inter- and intra-molecular hydrogen bonding.[189–192] In contrast, for PVDF and PPy, different interaction mechanisms dominate. In PVDF-based systems, dipole–dipole and weak electrostatic interactions between CQD surface functionalities and the polar C–F bonds of the polymer chain are prevalent.[193] In PPy/CQD systems, the interaction is primarily governed by π–π stacking between the conjugated pyrrole rings of PPy and the graphitic domains of CQDs.[194] These materials can form highly uniform, porous and flexible films while maintaining good compatibility with CQDs, making them ideal matrices for fabricating uniform, transparent, and mechanically robust fluorescent composite films.[8] As a result, these CQD-based thin films hold great potential for diverse applications, including environmental monitoring, biomedical sensing, optoelectronics, and food preservation. Different fabrication methods for CQD-based films are illustrated in Fig. 5.

3.1 Electrospinning

Electrospinning is a highly effective technique for fabricating nanofiber-based polymeric films.[195] To prepare CQD-based films using this technique, CQDs are first dispersed into a solution of polymers such as PVA, PVDF, PET or cellulose.[190,193,196] The resulting mixture is then loaded into a syringe. A charged jet of the polymer solution is generated under a strong electric field. As the jet moves toward a grounded collector, the solvent gradually evaporates, forming a non-woven mat of ultra-thin polymer fibers with uniformly embedded CQDs.

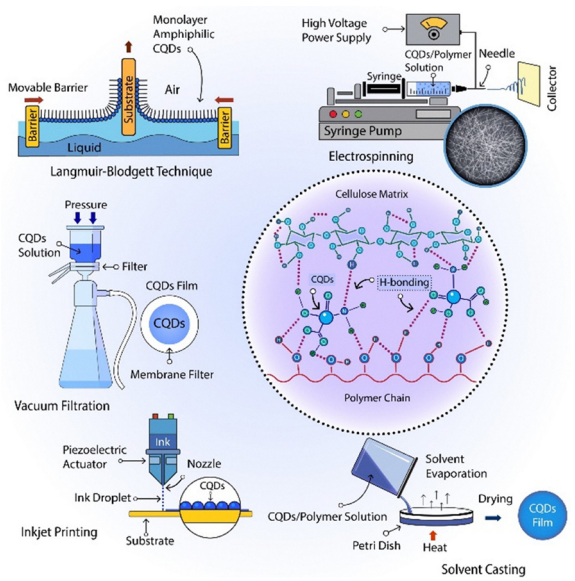

Fig. 5 Fabrication methods of CQD-based films.

Qin *et al.* reported a double-layer nanofiber film for *via* electrospinning food packaging and preservation applications.[197] The base substrate was formed from anthocyanin, soy protein isolate (SPI), and PVA. A separate layer was created by mixing CQDs with chitosan quaternary ammonium salt (HACC) and PVA, where –OH and –NH_2 groups in HACC formed hydrogen bonds with the –OH groups of PVA, enhancing chain entanglement and film stability. The CQD–polymer mixture was then deposited onto the anthocyanin-based substrate using electrospinning, resulting in a nanofibrous and active double-layer colorimetric film.

The electrospinning technique was also utilized to fabricate a dual-component nanofibrous scaffold for wound-healing applications.[198] Two separate polymer solutions were electrospun simultaneously, including a gelatin–chitosan solution containing silver-coated CQDs (Ag–CQDs) and citrate buffer and a polycaprolactone (PCL) solution. The Ag–CQD-integrated GCP scaffold (GCP-Q) and the citrate-modified GCP-Q scaffold (GCP-QC) thus produced exhibited enhanced wound-healing and anti-inflammatory properties.

In another study, a composite fluorescent amine sensor was fabricated *via* electrospinning for the real-time monitoring of food spoilage.[199] The sensor was developed as a composite nanofibrous film by electrospinning a solution of PVDF and CQDs derived from *p*-phenylenediamine. The resulting hydrophobic film exhibited a distinct fluorescence color shift from yellow-green to blue upon exposure to biogenic amines released from meat products within high-humidity packaging. Similar PVDF/CQD composite nanofibers were reported that exhibited piezoelectric and fluorescence properties.[200] There, CQDs with N–H and O–H functional groups and PVDF were first dissolved in a mixed solvent of DMF and acetone to prepare the precursor solution, which was then electrospun to produce nanofibers. The functional groups of the CQDs formed hydrogen bonds with the –CF_2 groups in PVDF, thus enhancing dipole alignment and β-phase content and contributing to the nanofibers' piezoelectric properties.

Nie *et al.* blended citric acid-derived CQDs with polyacrylonitrile (PAN) in *N*,*N*-dimethylformamide (DMF) to obtain a clear and homogeneous precursor solution.[201] This solution was then electrospun to produce nanofiber films that demonstrated low toxicity, excellent biocompatibility, and outstanding antibacterial efficiency (~99.99%) against *E. coli*, *P. aeruginosa*, and *B. subtilis*.

In another study, a dual-functional CQD/TiO_2 nanofiber membrane was fabricated using the electrospinning technique.[202] There, citric acid-derived CQDs were incorporated into TiO_2 and then mixed with a PI/PES solution to prepare the precursor for electrospinning. The membrane exhibited enhanced photocatalytic degradation of volatile

organic compounds such as acetone and excellent particulate filtration efficiency (>99%) for $PM_{0.1}$. The same material composition and electrospinning technique were employed to fabricate nanofiber membranes with strong antibacterial activity against both *E. coli* and *S. aureus*.[203]

Viscusi *et al.* fabricated nanofibrous membranes using the electrospinning technique.[204] In this work, nitrogen-doped CQDs were derived from pinewood sawdust and incorporated into a cellulose acetate (CA) solution to form the precursor. The resulting electrospun CA/CQD membranes exhibited significantly enhanced adsorption capacity for organic dyes, including methylene blue (MB) and methyl violet (MV), demonstrating the membranes' effectiveness in removing organic pollutants from wastewater.

3.2 Drop and solvent casting

Drop-casting and solvent-casting are simple and cost-effective techniques that are widely used for fabricating CQD-based composite films. In this process, CQDs are dispersed into a polymer matrix like PVA, cellulose, or chitosan. This resulting solution is deposited onto a substrate and a solid, and a freestanding composite film forms gradually as the solvent evaporates.

In one study, a simple solvent casting technique was used to fabricate an antibacterial membrane film.[192] In this work, nitrogen-doped CQDs (N-CQDs), synthesized from lemon pulp and urea, were dispersed into a PVA solution. This mixture was then poured into molds and allowed to dry at room temperature for 24 hours, thus forming a solid, freestanding composite film. The film exhibited high mechanical strength and strong antibacterial activity, which was attributed to the enhanced generation of ROS by the incorporated N-CQDs. Jaykumar *et al.* employed a solvent casting method to fabricate a CQD-incorporated PVA thin film, which exhibited near-complete UV-blocking properties. The films demonstrated potent antibacterial efficacy, achieving 100% inhibition against *S. aureus* and *S. enterica*, as well as a high antioxidant activity (~99%) as determined by the ABTS (2,2′-azino-bis(3-ethylbenzothiazoline-6-sulfonic acid)) assay.[205] In a similar work,[206] a UV-blocking film with antioxidant and antibacterial properties was fabricated by solvent-casting a solution of green tea-derived CQDs and PVA. Tao *et al.* fabricated a composite film by solution casting a uniform dispersion of lignocellulose-derived CQDs in a PVA matrix.[207] The resulting film demonstrated excellent mechanical flexibility, strong fluorescence, and sensitive pH-responsive behavior across a pH range of 4–8. A solvent casting technique was also employed to fabricate PVA/CQD nanocomposites that demonstrated both UV-blocking capability and photocatalytic activity for methylene blue degradation in wastewater.[191] Xu *et al.* also employed a solvent casting technique to fabricate PVA/cellulose nanofiber/CQD bionanocomposite films, which demonstrated strong fluorescence and effective UV-blocking capabilities.[208]

A transparent composite film was fabricated by casting a mixture of nitrogen and phosphorus co-doped CQD (N,P-CQD) and chitosan solution.[209] The resulting N,P-CQD/chitosan composite film exhibited high mechanical and thermal stability. The film showed strong antibacterial efficacy against *E. coli* and *S. aureus* along with excellent UV-blocking capabilities.

A solution casting method was used to fabricate CQD/furcellaran (FUR) nanocomposite films.[210] In this work, CQDs were added to a mixture of an aqueous furcellaran solution and glycerol plasticizer. The resulting solution was cast into Petri dishes and dried for 24 hours. The resulting films demonstrated enhanced radical scavenging, metal chelating, and UV-barrier properties as well as strong antimicrobial activity against *S. aureus* and *E. coli*.

A solvent casting technique was employed to fabricate a fluorescent PVA/CQD composite film.[211] After synthesizing coal-derived CQDs, they were mixed into a PVA solution. This PVA/CQD solution was then cast onto a glass substrate and dried under vacuum at room temperature to form a solid film, which exhibited strong blue emission. A transparent photoluminescent film was fabricated by casting an aqueous silk fibroin (SF) and CQD solution onto a polydimethylsiloxane (PDMS) substrate, followed by drying and methanol annealing.[212] The resulting SF-CQD composite exhibited enhanced PL, emitting strong green light (500–600 nm) under 380 nm excitation.

3.3 Vacuum filtration

While solution casting and electrospinning are widely reported in the literature, some studies have also employed vacuum filtration for film fabrication.[213,214] In this technique, a pressure differential created by an applied vacuum pulls the liquid phase through a porous filter medium, enabling the solid components to deposit uniformly onto the filter surface.[7,11,19]

A fluorescent film was fabricated by filtering a mixture of chitosan-derived CQDs and dialdehyde cellulose nanofibrils (DNF) through a 0.1 μm membrane.[215] Vacuum filtration was used to remove the liquid phase, leaving a homogeneous film with a thickness of 0.2 mm after drying. The film formed a dense internal network through Schiff base crosslinking between the CQDs and DNF, along with additional hydrogen bonding, which together improved its thermal stability and mechanical strength. The resulting composite film exhibited strong fluorescence and high sensitivity toward Fe^{3+} ions.

Khan *et al.* employed vacuum filtration followed by sequential compression molding to uniformly deposit a network of CQD–coupled cellulose nanofibers (CNFs) for fabricating a non-toxic, biocompatible air-filtration membrane.[214] The CNFs were first surface-modified *via* oxidation using 2,2,6,6-tetramethylpiperidine-1-oxyl (TEMPO) and then hydrothermally coupled with N/S-doped CQDs derived from palm-bunch biomass to obtain a mechanically robust composite film. The resulting membranes exhibited high filtration efficiency in capturing aerosol particles, thus demonstrating their potential as environmentally friendly, high-performance air-filtration materials.

Vacuum filtration was also employed to deposit and immobilize a CQD-based fluorescence-responsive sensing layer onto a glass-fiber membrane.[213] A suspension of sulfur-doped CQDs

(S-CQDs) and polydopamine (PDA) was vacuum-filtered, enabling the composite to uniformly assemble and firmly anchor onto and within the porous membrane structure. The resulting PDA-rich surface provided abundant adhesion sites for efficient microplastic capture, leading to enhanced retention of polyethylene (PE) microplastics with a significantly stronger fluorescence response.

3.4 Other techniques

Researchers have also employed various other techniques to fabricate CQD-based thin films. Among these, inkjet printing has emerged as a cost-effective method for precise deposition of CQD inks onto diverse substrates such as PVDF membranes and cotton fabrics.

A CQD-based hybrid photocatalytic film was fabricated by depositing an ink of *in situ* doped TiO_2(i)@CQD nanoparticles (T-CQD NPs) on a PVDF substrate using an inkjet printing method.[216] The resulting PVDF/TiO_2(i)@CQD film exhibited exceptional photocatalytic activity, owing to its S-scheme heterojunction structure and small particle size that collectively enhanced charge separation and electron transfer. Furthermore, the formation of Ti–F bonds between the nanoparticle catalysts and the PVDF substrate significantly improved the film's mechanical stability and reusability.

Kalytchuk *et al.* developed a security ink based on the tunable fluorescence lifetime of CQDs.[217] The ink was formulated by dispersing CQDs at various concentrations into PVA solution. The authors fabricated multiple anti-counterfeiting tags by applying the ink onto commercial non-fluorescent paper using various techniques, including inkjet printing, transfer printing, casting, and handwriting, thereby demonstrating the ink's versatility for different security marking applications.

In recent years, the Langmuir–Blodgett (LB) technique has gained significant attention for its capability to deposit highly ordered, defect-free ultrathin films with molecular-level precision.[218] In this method, amphiphilic molecules floating on the surface of a liquid are compressed at the air–liquid interface to form a closely packed, two-dimensionally ordered Langmuir monolayer. This monolayer is subsequently transferred onto a solid substrate through controlled vertical dipping to form Langmuir–Blodgett films. By repeating the deposition process, precise multilayer Langmuir–Blodgett films can be fabricated. Bodik *et al.* successfully fabricated a

Table 2 Comparative evaluation of CQD thin-film fabrication methods

Technique	Polymer matrices/ substrates	Scalability	Film morphology	Key advantages	Drawbacks
Solvent casting	PVA, PVP, PMMA, PPy, chitosan, cellulose	High	Flexible film	– Simple, low-cost equipment – Good optical transparency – Suitable for hydrophilic polymers	– Often requires toxic or flammable VOCs – Requires a polymeric binder
Inkjet printing	PVA, PVP, PEG, and PVDF	Moderate	Paper based film	– Easy to use, cost-effective – Scalable fabrication – Low material wastage – Mask free patterning	– Substrate is required – Ultra-small size, ~2–10 nm to prevent nozzle clogging – Limited viscosity range
Electro-spinning	PVA, PAN, PPy, CNF, PLA, and PET	Moderate	Porous membrane or film	– Extremely high surface area – Porous: ideal for sensing, filtration – High flexibility and mechanical strength – Substrate-free film formation	– Needs high power supply – Low production rate – Limited types of substrates – High degree of defect formation
Vacuum filtration	Cellulose, PVDF	Moderate	Flexible film	– Simple, low-cost equipment – Fast processing – Good for creating flexible CQD films	– Low-viscosity solvent requirement – Non-uniform thickness – High aggregation tendency
Spin coating	PMMA, PDMS, FTO, ITO, and glass	Low	Solid film	– Cost-effective and rapid processing – Uniform thin film formation – Low deposition temperature	– Low material efficiency – Restricted to planar substrates – Limited by substrate size
Langmuir–Blodgett	CQDs with hydrophobic ligands and silicon	Low	Solid film	– Ultimate control over film thickness – Creates defect-free, ultra-thin films	– Transfer process may introduce defects, particularly in soft or structurally unstable molecular films

FTO: fluorine-doped tin oxide; ITO: indium tin oxide; PET: polyethylene terephthalate; PLA: polylactic acid; PMMA: poly(methyl methacrylate); PPy: polypyrrole; PVA: poly(vinyl alcohol); PVDF: poly(vinylidene fluoride); PVP: polyvinylpyrrolidone; VOCs: volatile organic compounds.

monolayer LB film of hydrophobic CQDs (hCQDs) on a silicon substrate.[219] The resulting film exhibited strong PL and high structural integrity, demonstrating the effectiveness of the LB technique for producing uniform monolayer CQD films.

The LB technique was also used to deposit uniform and homogeneous thin films of fluorescent, hydrophobic CQDs onto various substrates.[220] The resulting films demonstrated notable antibacterial and antifouling activities, particularly under blue-light irradiation. Table 2 presents a comparative assessment of different fabrication methods for CQD thin films.

4 Functional applications of CQD-based films

4.1. Sensing and monitoring

Carbon quantum dots (CQDs) offer tunable optoelectronic properties and can be functionalized with diverse chemical groups, making them a versatile nanomaterial for fabricating sensing and detection platforms through integration into polymeric films (Fig. 6). These thin, often flexible films can be engineered to detect subtle changes in the concentration of biochemicals, toxic gases, and environmental pollutants through measurable electrochemical and fluorescence responses.

4.1.1 Chemical sensors

4.1.1.1 Heavy metal ions. Carbon quantum dot (CQD)-based thin films have been widely used for detecting heavy metals in water. The interaction between the metal ions and the CQDs induces measurable changes in the fluorescence emission, thus allowing for the quantitative analysis of heavy metal contaminants.

For example, a fluorescence-based lead (Pb^{2+}) sensor was fabricated by embedding dithizone-functionalized CQDs within a chitosan thin film.[221] When coupled with a fiber optic spectrometer (FOS), the sensor exhibited a highly accurate linear response across the 0–100 μM concentration range, achieving a detection limit of 18.3 nM with a rapid response time (<60 s) and a maximum error of ~1.4% in water samples.

In a separate study, they introduced a CQD-based thin film for fluorescence-based detection of heavy metals in water.[222] The CQDs were synthesized from folic acid and incorporated into a PVA matrix to form the sensing film. The sensor demonstrated highly accurate performance in detecting heavy metals (Pb, Ni, Mn, Co, and Cr) with a linear detection range of 0–100 μM, a rapid response time below 60 seconds, and low detection limits ranging from 0.006 to 0.019 ppm in real water samples. The reported sensors thus offer a fast, sensitive, and reliable point-of-care platform for monitoring heavy metal contamination in water sources.[221,222]

An electrochemical sensor was developed for detecting lead ions (Pb^{2+}) using CQD-based thin films.[223] The CQDs were synthesized from glutathione (GSH) and integrated with poly(allylamine hydrochloride) (PAH) *via* a layer-by-layer (LBL) assembly technique. The GSH ligand functionalizes the CQDs with sulfhydryl (–SH) groups, creating specific binding sites for Pb^{2+} ions. Furthermore, the branched structure of the PAH matrix significantly increases the film's active surface area, thereby enhancing sensor sensitivity by increasing the interaction between the CQDs and Pb^{2+} ions while facilitating more efficient electron transfer.

Vyas *et al.* developed a CQD-based thin-film sensor for detecting mercury (Hg^{2+}) in water.[224] The film was fabricated by incorporating CQDs and diphenyl carbazone (DPCO) into a chitosan (CS) polymer matrix. When exposed to Hg^{2+} ions, DPCO forms a violet-colored complex, enabling colorimetric detection using a smartphone camera. This binding also releases protons, thus altering the pH of the medium. The change in pH affects the fluorescence of the CQDs, enabling simultaneous fluorometric detection of mercury in water. The authors reported achieving limits of detection (LoD) of 290 ppb and 1.8 ppb for colorimetric and fluorometric sensing, respectively.

A CQD–dimethylglyoxime (CQD–DMG) composite thin film was fabricated for rapid detection of Ni^{2+} ions in water.[225] The sensor demonstrated 95% accuracy compared to standard spectroscopic analysis with low detection limits (0.36 ppm optical and 0.29 ppm electrochemical) and faster response (<1 minute), thus making the dual sensing platform suitable for rapid, on-site detection of Ni^{2+} in water resources.

4.1.1.2 Organic molecules and gases. In one study, an electrochemical dopamine (DA) biosensor based on a CQD and chitosan (CS) composite film was reported.[226] The sensitivity of the sensor was enhanced by depositing the composite film on a glassy carbon electrode. The sensor exhibited a linear response across a DA concentration range of 0.1–30.0 μM and a low detection limit of 11.2 nM, making it a promising tool for clinical diagnostics and pharmaceutical analysis.

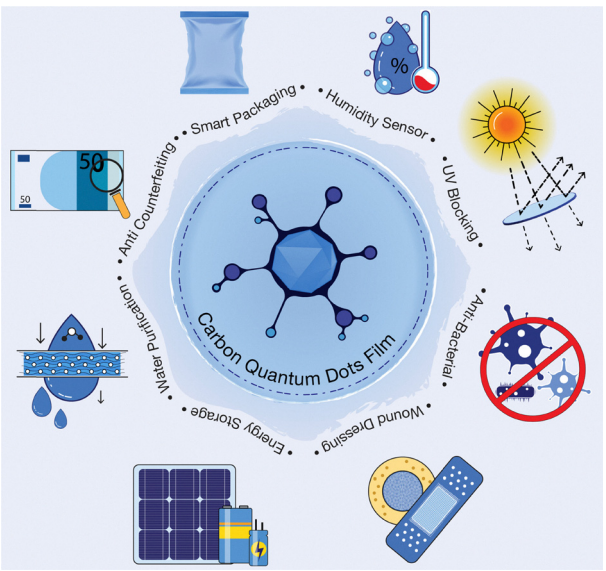

Fig. 6 Applications of CQD-based films.

Vyas *et al.* reported a CQD-based thin film biosensor for detecting organophosphorus pesticides, specifically ethyl paraoxon (EP) and methyl parathion (MP), in water samples.[227] The CQDs were synthesized *via* a one-pot hydrothermal method using phthalic acid and triethylenediamine. The CQDs were then incorporated into a chitosan film, onto which recombinant organophosphorus acid anhydrolase (OPAA) enzyme was immobilized to realize the sensor. The sensor exhibited a linear detection range of 0–100 μM for both pesticides, with detection limits of 0.18 ppm for EP and 0.69 ppm for MP. With a response time below five minutes, these sensors thus allow for rapid and accurate on-site analysis of organophosphate contamination in real water samples.

A CQD-based thin film sensor was fabricated for formaldehyde vapor detection.[228] The CQDs were synthesized from laurel leaves and embedded into a PPy film. The CQD/PPy nanocomposite film thus produced was coated onto a quartz-crystal microbalance (QCM) electrode to fabricate the sensor. The sensor demonstrated high linearity and sensitivity across a low formaldehyde concentration range of 0.58–5.82 mg L^{-1} while exhibiting good selectivity, reproducibility, and stability, thus making the sensor a viable and reliable solution for indoor air quality monitoring and environmental safety applications.

Ren *et al.* developed a fluorescence-based sensor for toluene gas detection using nitrogen-functionalized CQDs (N-CQDs), where the nitrogen functional groups enable the CQDs to form specific hydrogen bonds with toluene molecules.[229] The CQDs were synthesized through a hydrothermal reaction of glycerol and betaine and then incorporated into a carboxymethyl cellulose (CMC) membrane. The resulting composite exhibited high selectivity for toluene, demonstrating a linear fluorescence response across a concentration range of 200–1400 ppm with a detection limit of 0.452 ppm.

4.1.2 Environmental monitoring sensors. A humidity-sensitive composite was developed by incorporating CQDs into nanofiber clusters (CQDs@NFCs) through a wafer-level plasma etching and solvent evaporation process.[230] The authors used this composite to fabricate a flexible humidity sensor. The sensor exhibited over a four-fold increase in fluorescence-based sensitivity across the 7% to 59% relative humidity (RH) range, which the authors attribute to the composite's large surface area and abundance of hydrophilic functional groups.

Liu *et al.* developed a temperature sensor based on red-emitting CQDs (R-CQDs) synthesized from *o*-phenylenediamine (*o*PD).[231] The derived R-CQDs were incorporated into a PVA matrix to form a composite film. The film exhibited pronounced temperature-dependent fluorescence at low temperatures (190–260 K) with a relative sensitivity of 0.62% per K, thus making it a viable choice for non-contact temperature sensing in cryogenic applications. Elsewhere, a highly sensitive and stable temperature probe was fabricated from a tunable fluorescent film.[232] The film was composed of methylated CQDs in a PVA matrix, exhibiting red-emission with a linear thermal response ($R^2 > 0.99$) across a wide temperature range (20–60 °C). The sensor also maintained high signal reversibility over at least four heating–cooling cycles between 20 and 80 °C.

A temperature-dependent fluorescent film was fabricated using CQDs derived from lemon bagasse extract.[233] The film further demonstrated significant antioxidant properties. Sun *et al.* reported achieving tunable PL (ranging from blue to green and red) and temperature-sensitive properties in methylenated CQD/PVA films by systematically modifying surface functional groups (–NH_2, –OH, –COOH, and –CH_2OH) *via* a direct hydrothermal synthesis process.[232] The CQDs were synthesized within a Teflon-lined stainless-steel autoclave at 180 °C through a direct hydrothermal reaction of citric acid (CA) and diethylenetriamine (DETA) mixed in a specific molar ratio. The resulting CQDs were then incorporated into a PVA matrix to fabricate temperature-sensitive composite films for optical temperature probes. In a similar work,[234] a CQD/PVA composite-based optical temperature sensor exhibited a strong linear response ($R^2 > 0.99$) across the 20–90 °C range with a relative thermal sensitivity of 2.84% per K.

A functionalized glass-fiber membrane was fabricated to capture and detect microplastics.[213] The membrane's active layer was fabricated by incorporating sulfur-doped CQDs (S-CQDs) and polydopamine (PDA) *via* vacuum filtration. This created a surface rich in adhesive PDA, which efficiently captured polyethylene (PE) microplastics. The incorporated S-CQDs provided a strong fluorescence signal upon capture, enabling the visual detection and retention of the microplastics with significantly enhanced sensitivity.

4.2 Water treatment and ion filtration

Carbon quantum dots (CQDs), when appropriately functionalized, exhibit excellent water solubility and uniform dispersibility in various polar solvents, such as ethanol, methanol, and ethylene glycol. Furthermore, these surface-functionalized CQDs integrate effectively within polymer matrices.[235] The resulting CQD-based composites often demonstrate photocatalytic activity. When exposed to sunlight, these composites generate ROS, which effectively degrade organic pollutants and inactivate bacterial contaminants.[236]

When incorporated into filtration membranes, CQDs modify the porous structure to achieve highly selective and efficient removal of contaminants.[236,237] Furthermore, the functionalization of CQDs with hydrophilic groups such as hydroxyl and carboxyl enables them to attract water molecules through hydrogen bonding, which significantly enhances membrane permeability and flow efficiency.[9] These tailored properties make CQD-based films cost-effective and environmentally sustainable materials for applications in water treatment and desalination.[238,239]

A CQD-based thin-film nanocomposite (TFN) hollow fiber membrane was developed for water desalination applications.[240] The TFN was fabricated by incorporating sodium-functionalized CQDs (Na-CQDs) into polyamide (PI) through an interfacial polymerization reaction. The Na-CQDs not only increased the membrane's effective surface area but also created more interstitial spaces within the PI matrix, thereby significantly enhancing its water permeability

compared to conventional thin-film composite membranes, while maintaining over 97.5% salt (NaCl) rejection efficiency.

Sun *et al.* synthesized various surface-functionalized CQDs and fabricated thin-film nanocomposite membranes by incorporating them into the PI layer using an interfacial polymerization technique.[241] The sulfonic acid-functionalized CQD membrane exhibited significantly enhanced water permeation with 93.6% Na_2SO_4 rejection, whereas the amino-functionalized CQD membrane demonstrated superior anti-fouling performance.

Another study reported the fabrication of several hybrid organic solvent nanofiltration (OSN) membranes by incorporating sub-5 nm CQDs into a PEI matrix.[242] The surface functional groups of the CQDs were tuned through precise control of the carbonization degree during synthesis. This PEI/CQD composite was then coated onto a polyacrylonitrile (PAN) substrate to form a thin active layer. The resulting membranes exhibited high durability and solvent resistance, which was attributed to the fully cross-linked PEI network. Notably, the incorporation of lowly carbonized CQDs facilitated the permeation of polar solvents, achieving a 54.3% increase in isopropanol permeance, while simultaneously suppressing the transport of non-polar solvents, thereby significantly improving membrane selectivity.

Yang *et al.* demonstrated that the incorporation of zwitterionic CQDs into a cellulose acetate/thermoplastic polyurethane (CA/TPU) matrix significantly increased the membrane's pore size, porosity, and surface roughness.[243] These enhanced properties resulted in high pure water flux, a 95.4% copper ion rejection rate, and superior anti-fouling performance, demonstrating the material's strong potential for large-scale, industrial wastewater treatment applications.

4.3 Photonic and electronic applications

Carbon quantum dot (CQD)-based films function as highly efficient active layers in electrochromic devices due to their tunable and highly stable optical and electrical properties.[244] Their high surface area, excellent electrical conductivity, and rich surface chemistry facilitate rapid charge transfer and efficient redox reactions, enabling faster coloration/bleaching switching at low driving voltages.[1,245] These properties make CQD-based films particularly well-suited for advanced applications in smart windows, flexible displays, and other dynamic optical filters.

4.3.1 Light emission. To enhance the electrochromic performance of polyaniline (PANI) films in the infrared region, Qin *et al.* synthesized a CQD-embedded porous PANI film on a gold-coated polyethersulfone (Au/PES) substrate *via* an electrochemical polymerization process.[246] The oxygen-containing functional groups on the CQDs form hydrogen bonds with the PANI chains that induce localized deformations, thus promoting a porous morphology. The optimized PANI/CQD composite demonstrated an optical contrast (ΔT) of 53% at 850 nm and substantial thermal emittance modulation ($\Delta\varepsilon$ = 0.41–0.46) across the 2.5–25 μm spectral band. The composite also showed improved switching kinetics and superior cycling stability over pure PANI films, thus making it a promising material for advanced flexible electrochromic devices.

Another study reported the synthesis of nitrogen- and sulfur-co-doped CQDs (N,S-CQDs) from discarded cigarette butts *via* a hydrothermal process.[247] The resulting CQDs exhibit bright and stable fluorescence, making them a sustainable and cost-effective nanomaterial suitable for multiple applications including bioimaging, security inks, anti-counterfeiting, and sensing. When incorporated into a PVA matrix, the CQDs formed highly photostable fluorescent films, demonstrating strong potential for use in optical and optoelectronic devices such as fluorescent displays and light-emitting diodes (LEDs).

4.3.2 Photodetection. A CQD-based ultraviolet (UV) photodetector was reported, where mango leaf-derived CQDs were chemisorbed onto zinc oxide nanorods (ZnO-NRs) to form thin-films of a CQD/ZnO-NR heterostructure.[248] The resulting device outperformed conventional ZnO-based UV detectors, achieving a photocurrent density of 123.49 μA cm^{-2}, a responsivity of 81.2 mA W^{-1}, and an external quantum efficiency (EQE) of 27.6% at 1 V under 365 nm illumination (1 mW cm^{-2}). The device also exhibited an enhanced zero-bias photoresponse compared to pristine ZnO nanorod-based devices, thus enabling self-powered operation.

Thyda *et al.* fabricated highly transparent (>95%) CQD-incorporated hybrid thin films for UV detection using a spin-coating technique.[249] The hybrid structure was formed by adsorbing nitrogen-doped CQDs onto ZnO crystallites to regulate the ZnO particle size, thereby enhancing the film's quality and signal-to-noise ratio (SNR). The resulting photodetector exhibited stable and reproducible performance under 365 nm UV illumination (1 mW cm^{-2}), demonstrating nearly threefold higher responsivity and external quantum efficiency (EQE) while substantially reducing the dark current compared to pristine ZnO-based devices.

4.3.3 Memory devices. Carbon quantum dot (CQD)-based films can potentially be a cost-effective platform for the development of flexible wearable memory devices. For example, a composite resistive memory device was fabricated by incorporating CQDs into a Co_3O_4 thin film.[250] The CQDs enhance the electric field locally, thus promoting the controlled formation of confined conductive filaments and thereby improving resistive switching uniformity. Furthermore, variations in oxygen vacancy concentration cause reversible conversion between Co^{2+} and Co^{3+} oxidation states, thus modulating the magnetic properties of the material. The composite device demonstrated superior performance compared to its pristine Co_3O_4 counterpart, exhibiting a lower initialization voltage, reduced variability in set/reset voltages, and improved retention stability. Furthermore, the device showed significant magnetization modulation (~57%), with saturation magnetization (M_s) values of 49, 95, and 113 emu cm^{-3} corresponding to the initial, high-resistance, and low-resistance states, respectively. These properties make this material promising for developing multifunctional electro-magnetic integrated systems and next-generation non-volatile memory.

4.3.4 Smart materials. A luminescent shape-memory polymer (SMP) composite film was fabricated by blending cellulose-derived CQDs with PVA.[251] The oxygen- and hydrogen-rich CQDs physically cross-link with the PVA matrix through hydrogen bonding, thereby inducing shape-memory properties. The composite exhibits a visibly traceable, full shape recovery at room temperature, with a recovery rate that can be adjusted from 20 to 200 seconds by modifying pH and temperature. This luminescent PVA/CQD SMP film thus has potential applications in smart medical devices, stimuli-responsive drug release systems, and intelligent flexible sensors.

4.4 Energy storage and conversion

The incorporation of CQDs into flexible films significantly enhances their electrical conductivity and charge storage capacity, making them excellent candidates for fabricating high-performance, robust, and flexible supercapacitors. CQDs improve the specific capacitance and energy density of these composite films by facilitating electron transport and increasing the number of active sites available for redox reactions. Furthermore, CQDs can act as binders or spacers within the film's matrix while enhancing its specific surface area, mechanical flexibility, and porosity. As CQD-based composite films can effectively buffer volume changes during charge–discharge cycles and preserve electrode's structural integrity, they frequently exhibit excellent long-term charge retention over thousands of cycles.[194,252–254]

In one study, a CQD/PPy-based composite film was developed utilizing a direct electrochemical technique to fabricate a flexible all solid-state supercapacitor (ASSS).[194] The device exhibited excellent cycling stability, retaining 85.7% of its initial capacitance after 2000 charge–discharge cycles. Furthermore, the ASSS achieved an areal capacitance of 315 mF cm^{-2} at a current density of 0.2 mA cm^{-2}, thus demonstrating its potential for flexible energy storage applications.

Dhandapani *et al.* employed a hybrid electrospray deposition technique to fabricate high-performance composite thin film electrodes for supercapacitor applications, where CQDs were anchored within a poly(aniline-*co*-indole) copolymer matrix.[254] The fabricated thin film electrode exhibited excellent cycling stability with a maximum specific capacity of 185.1 C g^{-1} at a current density of 2 A g^{-1}, while retaining 79.4% of its capacity at a high current density of 20 A g^{-1} after 10 000 consecutive charge–discharge cycles. In a separate study, a PPy/CQD composite thin film was synthesized by incorporating CQDs into PPy *via* a hybrid electrospray technique.[255] The study reported a specific capacitance of 79.25 C g^{-1} at a current density of 1.5 Ag^{-1}, with an energy density and power density of 26.44 Wh kg^{-1} and 18 090.82 W kg^{-1}, respectively. The authors used the composite to fabricate all-solid-state asymmetric supercapacitor devices. These supercapacitors thus produced demonstrated an excellent cyclic retention rate of 76.8% over 10 000 cycles at a high current density of 15 A g^{-1}, thus making the PPy/CQD composite film a promising material for semi-flexible energy storage applications.

Elsewhere, CQD films were deposited on N_2 plasma-treated carbon cloth *via* electrodeposition.[256] The resulting electrode exhibited significantly enhanced performance due to electrochemical activation, achieving 572.5 mF cm^{-2} areal specific capacitance and 2862 F g^{-1} mass specific capacitance. The authors fabricated a solid symmetrical supercapacitor using the prepared CQD films. There they reported achieving an energy density of 17.04 μWh cm^{-2} at a power density of 200 mW cm^{-2}, thus demonstrating its potential for efficient energy storage applications.

The light absorption characteristics of CQDs can be engineered by modifying their electronic bandgap through precise control of their size and surface chemistry.[91,108,161] Furthermore, CQD films can be fabricated with high electrical conductivity, which facilitates efficient charge transport in electronic devices.[257] These properties of CQD-based films thus allow for the fabrication of lightweight, flexible photovoltaic devices suitable for wearable devices.

Maxim *et al.* developed a sandwich-structured perovskite solar cell (PSC) incorporating a phosphorus-doped CQD layer.[258] The CQDs were embedded in a thin poly(methyl methacrylate) (PMMA) film and applied on the device's illuminated surface to enhance light harvesting. This layer converts high-energy ultraviolet (UV) light into visible wavelengths, thereby compensating for optical losses in the perovskite absorber and resulting in an ∼3% increase in photocurrent and a fill factor improvement of ∼6%. Another study reported the synthesis of silicon-functionalized CQDs (Si-CQDs) using a one-step hydrothermal method and integrated them into a PVA matrix to fabricate Si-CQDs@PVA composite thin films.[259] These films functioned as luminescent downshifting (LDS) layers in cadmium telluride (CdTe) photovoltaic cells, resulting in an increase of the short-circuit current density from 0.82 to 0.84 mA cm^{-2} with a 4.76% improvement in power conversion efficiency.

4.5 Security applications

A CQD-based fluorescent security ink was developed for anti-counterfeiting applications.[217] The fluorescent CQDs were synthesized by reacting citric acid (CA) with EDA and subsequently blended into a PVA solution to produce a fluorescence lifetime-based, non-toxic ink for security applications. Ren *et al.* proposed a scalable synthesis method for CQDs using a vacuum heating technique.[255] The resulting CQDs were incorporated into polymers to create multicolor fluorescent security ink. When printed on cotton fabric, the ink maintained a quantum yield of 42%, making it a promising candidate for high-performance, flexible anti-counterfeiting applications.

In one study, fluorescent CQD-based composites were developed for anti-counterfeiting applications.[260] The composites were prepared *via* vacuum heating of a precursor mixture containing citric acid, urea, boric acid, and $CaCl_2$, as well as by dispersing CQDs in polyvinylpyrrolidone (PVP) or an aqueous solution of cyanic acid. These green-fluorescent CQD-composite materials were then directly mixed with ethanol to produce a fluorescent ink. The CQDs thus obtained exhibited

high QY (40–67%) and strong temperature-dependent fluorescence, making them suitable for flexible and temperature-responsive security encoding, anti-counterfeiting, and optical encryption.

To promote environmental sustainability, Park *et al.* synthesized fluorescent CQDs from municipal wastepaper as a low-cost and eco-friendly precursor. They employed a conventional solvothermal method using various solvents, including water, ethanol (EtOH), and 2-propanol (PrOH), to process the waste material. The resulting CQDs exhibited strong fluorescence, as well as excellent chemical and photostability, making the synthesized CQDs a sustainable solution for applications in anti-counterfeiting and flexible displays. In another sustainable approach,[261] fluorescent CQDs were synthesized from hydrolyzed lignin and EDA in formamide (FA) precursors *via* a hydrothermal reaction. The resulting CQDs exhibit strong blue fluorescence along with high thermal and aging stability, making them a promising sustainable material for fabricating fluorescent films and anti-counterfeiting inks.

4.6 Active food packaging

Carbon quantum dot (CQD)-based films are emerging as a smart and sustainable solution for food packaging. These films can be synthesized from various biomass and agricultural waste sources, such as fruit peels and cellulose, providing an eco-friendly alternative to conventional plastics.[262–264] The optical bandgap of CQDs can be tuned by controlling their size and surface chemistry during synthesis.[9] This tunable bandgap of CQDs enables the fabrication of films that effectively block harmful UV radiation while remaining highly transparent to visible light. These films can be engineered to enhance water vapor barrier properties, as well as exhibit antibacterial and antioxidant activities, evaluated by ABTS and 2,2-diphenyl-1-picrylhydrazyl (DPPH) radical scavenging assays. These CQD-based films thereby offer a sustainable packaging solution for food preservation and shelf-life extension.[265]

Metal and metal oxide-decorated CQD films have emerged as a promising class of materials for active food packaging. The synergistic interaction between the CQDs and the metallic components enhances the composite's antimicrobial and antioxidant strengths, making them viable for advanced food preservation applications. For instance, Na *et al.* fabricated a biopolymer-based film by incorporating zinc oxide (ZnO) and a ZnO/CQD nanocomposite into an agar matrix.[266] The resulting composite film demonstrated strong antibacterial and antioxidant efficacy, highlighting its potential as a sustainable packaging material to extend food shelf life and enhance food safety. Elsewhere, Ag-doped nitrogen-functionalized CQDs (Ag-NCQDs) were integrated with few-layered MoS_2 nanosheets to form a thermally stable MoS_2–Ag–NCQD composite.[267] When incorporated into a PVA matrix, the resulting film showed an extremely high oxygen barrier (99.8%) compared to pure PVA films, making the composite a promising candidate for active and intelligent packaging materials for the food and pharmaceutical industries.

Li *et al.* developed shielding films against ultraviolet (UV) and high-energy blue light (HEBL) by incorporating CQDs into a PVA matrix.[268] The CQDs were synthesized from hyperbranched PEI (hPEI) and hydroxybenzaldehyde derivatives using a solvothermal method. The resulting CQD/PVA composite films demonstrated high-performance optical shielding, with UV-blocking efficiency exceeding 98%, HEBL-blocking efficiency over 85%, while maintaining a transmittance of up to 70% for visible light. In a similar work, lignin-derived CQDs (L-CQDs) were incorporated into a PVA matrix to create an L-CQD/PVA film, which demonstrated effectively total blocking efficiency ($>99.9\%$) across the entire UV spectrum (UV-C, UV-B, and UV-A) and HEBL.[269]

Another study reported an active UV-blocking packaging film by integrating amine-functionalized CQDs into a TEMPO-oxidized nanocellulose (NC) matrix.[270] The resulting composite films exhibited near-complete UV-blocking efficiency ($\sim 99.8\%$), along with reduced water vapor permeability, enhanced mechanical strength (1.6 MPa), and high thermal resistance (330 °C), making the material an efficient and sustainable solution for food packaging. Ahmadi *et al.* incorporated CQDs into a polyurethane (PU) matrix to form a CQD–PU composite coating.[271] This composite demonstrated high UV stability, showing a 66% reduction in UV-induced chemical degradation in PU.

Many researchers explored organic and renewable sources, including various forms of biomass and agricultural waste, such as jute, coconut husk, banana pseudostems, and water hyacinth fibers, to synthesize CQD composite films.[267]

A biocompatible active film was fabricated by incorporating chitosan-derived CQDs into a carboxymethyl cellulose (CMC) polymer matrix.[272] The resulting composite film exhibited a 27.6% increase in tensile strength (TS) compared to the neat CMC film, along with high transparency and strong UV-blocking capability. Furthermore, the CQD–CMC film showed notable antibacterial and antifungal activities, as well as excellent antioxidant activity, with ABTS and DPPH radical scavenging efficiencies of 100% and 87–88%, respectively, contributing to the extended shelf life of lemons.

A guar gum/sodium alginate biopolymer film incorporated with lemon-derived CQDs demonstrated enhanced functional properties, including improved UV-blocking capability and a mechanical strength of 38.80 MPa.[273] The composite film also exhibited significant antioxidant activity, with ABTS and DPPH radical scavenging efficiencies of 92.4% and 86.6%, respectively, at 512 μg mL^{-1}, along with strong antibacterial efficacy, collectively contributing to delayed browning of blanched asparagus. Han *et al.* synthesized CQDs through a hydrothermal process using a precursor combination of lemon extract and ethyl acetate (EA).[91] These CQDs were subsequently embedded into a polylactic acid (PLA) matrix to fabricate nanocomposite films. The resulting PLA/CQD composite demonstrated excellent UV-B blocking capability and significant antimicrobial activity, making it a promising and cost-effective material for food preservation applications. In another study, an eco-friendly nanocomposite film for

active, biodegradable packaging was developed by incorporating lemon peel-derived CQDs into a PVA matrix.[205] The resulting composite film exhibited multiple functionalities, including antibacterial, antioxidant, and UV-shielding properties.

Ansari *et al.* developed transparent packaging films with UV-blocking and oxygen-barrier properties for food preservation and packaging applications.[206] There, they synthesized CQDs from green tea extract and incorporated them into a PVA matrix through a solvent casting technique to fabricate the functional films. Elsewhere, a bio-composite film was developed from CQDs and sericin protein using an ultrasound-assisted synthesis method.[274] The composite exhibited strong fluorescence, antibacterial, antioxidant, and UV-shielding properties. When applied as a coating it effectively preserved fresh-cut vegetables by inhibiting microbial growth and oxidative damage, thereby extending shelf life.

A low-cost, biocompatible packaging film was developed by incorporating glucose-derived CQDs into a chitosan/gelatin (Chi/Gel) polymer matrix.[275] The resulting Chi/Gel/CQD composite film exhibited strong UV-blocking, as well as enhanced ABTS and DPPH scavenging and antimicrobial properties. The film was reported to extend the shelf life of avocados by more than 14 days through the inhibition of mold growth. An active packaging film with light-conversion capability was fabricated by incorporating glucose-derived CQDs into a pectin matrix.[276] The composite film demonstrated photoluminescent down-conversion, transforming ultraviolet radiation into blue light. The ROS generated by the film contributed to strong antibacterial activity against *L. monocytogenes* and *E. coli*. The film also exhibited significant ABTS and DPPH radical scavenging efficacy and antifungal activity, achieving complete inhibition of the fungus *A. flavus*.

In one study, a series of active chitosan films reinforced with turmeric-derived CQDs were reported.[277] There, the fluorescence properties of the CQDs were used to achieve photodynamic inactivation of bacteria. Upon exposure to 405 nm light, the composite film generated a substantial amount of ROS, resulting in significant bactericidal activity. The authors reported a reduction in viable counts of *S. aureus* and *E. coli* by approximately 3.19 and 2.05 $\log_{10}$ CFU mL^{-1}, respectively, within 40 minutes, thus demonstrating the material's potential for application in antimicrobial food packaging.

A flexible and transparent CQD-based polymeric film was fabricated, which exhibited effective UV-blocking properties, along with strong antioxidant activity as demonstrated by ABTS and DPPH radical scavenging.[278] The film was fabricated through a simple mixing and casting process, where a thermoplastic starch (TPS) polymer was first synthesized from glycerol and starch and integrated with clove-derived CQDs and κ-carrageenan to form a CQD-based TPS/κ-carrageenan composite. The resulting composite exhibited high mechanical strength and stability, along with strong antioxidant activity, effective water vapor barrier properties, and low moisture retention. These properties make the composite a promising sustainable, eco-friendly, and biodegradable alternative to conventional food packaging, capable of extending the shelf life of agricultural products.

A zinc-doped CQD (Zn-CQD) composite film was developed as an active food packaging material with antibacterial and UV-protective properties.[279] The Zn-CQDs were synthesized through a hydrothermal process using crayfish shells and zinc acetate dihydrate as precursors. These quantum dots were subsequently incorporated into a PVA matrix to form the composite film. When tested on mangoes, the Zn-CQD/PVA film effectively extended their shelf life by maintaining fruit quality over a longer storage period.

Hong *et al.* synthesized Zn-CQDs from grapefruit peel and incorporated them into a CNF matrix to fabricate an antibacterial composite film (CNF/Zn-GFP-CQDs).[280] The film exhibited significant antibacterial activity against both Gram-positive and Gram-negative bacteria, limiting bacterial growth to below 7 $\log_{10}$ CFU g^{-1} over a two-week period. Furthermore, the composite film functioned as an effective UV barrier and demonstrated pronounced antioxidant capacity through efficient scavenging of ABTS and DPPH radicals, consequently reducing lipid oxidation.

A CQD-incorporated antibacterial composite film was developed based on starch and hyaluronic acid (HA).[281] The film was first modified with halloysite nanotubes pre-loaded with antibacterial malva extract. Subsequently included CQDs act synergistically with these natural antibacterial compounds to further enhance the film's antibacterial efficacy while simultaneously improving its structural flexibility. In antibacterial assays, the film demonstrated zones of inhibition (ZOI) of 0.4 ± 0.1 cm and 0.3 ± 0.1 cm against *S. aureus* and *E. coli*, respectively. Furthermore, the composite film exhibited improved cytocompatibility, thus validating its effectiveness in maintaining high cell viability.

4.7 Biomedical applications

Carbon quantum dot (CQD)-based films possess a unique combination of functional properties, including potent antimicrobial activity, significant antioxidant capacity, effective UV blocking, high biocompatibility, and enhanced wound healing capabilities.[57,73,138,265,272] When applied directly to wounds, these films function as a protective barrier that actively inhibits bacterial growth. Furthermore, they can be engineered for controlled therapeutic release and to promote cellular proliferation, thereby significantly accelerating wound healing.[21,157] Their inherent fluorescence properties also enable real-time, colorimetric monitoring of the wound site and facilitate cell labeling applications. This combination of functionalities makes CQD-based films a highly promising candidate for a wide variety of biomedical applications.

4.7.1 Wound healing. Carbon quantum dot-based films demonstrate strong broad-spectrum antimicrobial activity,[69,91,129,180,267] significant antioxidant capacity,[205,210,265,272] effective UV blocking,[209,268,270,273] high biocompatibility,[7,9,11,28] and enhanced wound healing capabilities,[123,146,282,283] especially after surface modification and exposure to visible light. The surface properties of CQDs influence their solubility, electrostatic

interaction with microbial membranes, and ROS generation.[279] These factors enhance the ability of CQD films to inflict oxidative damage on microbial biomolecules and cellular components.[284] Their versatility, capacity to inhibit biofilm formation, and effectiveness against both Gram-positive and Gram-negative bacteria make them highly promising candidates for next-generation wound dressings, especially in the treatment of complex or infected chronic wounds.

In one study, a chitosan (CS) hydrogel was used to develop an antimicrobial film for wound healing applications.[285] The CS hydrogel was plasticized with glycerol and crosslinked with folic acid-derived CQDs. When loaded with antibiotic gentamicin, the film exhibited a controlled release for up to 48 hours in a phosphate-buffered saline (PBS) medium. The CS/CQD composite film exhibited superior antibacterial performance compared to pure CS film, demonstrating a significantly enhanced ZOI of 2.5 ± 0.1 cm. Furthermore, cytotoxicity assays on human skin fibroblast cell lines confirmed the film's high biocompatibility, with cell viability exceeding 80%.

Wen *et al.* derived CQDs from ginger and incorporated them into a PVA/chitosan film.[282] The composite film exploited the photoresponsive properties of CQDs to enhance antibacterial efficacy and promote wound healing. When activated with light, the film efficiently generated ROS, thus significantly enhancing bacteriostatic activity and accelerating wound healing.

Another study reported an antibacterial composite film for wound healing applications,[283] where a hydrothermal technique was used to incorporate lanthanum-doped, nitrogen-phosphorus-*co*-doped CQDs (La@N-P-CQDs) into a PVA matrix. The La@N-P-CQD/PVA composite film exhibited antibiotic fluorescence, improved antibacterial activity, and accelerated wound healing, while showing no adverse effects *in vivo*, making it a promising candidate for advanced wound dressing.

Ezati *et al.* prepared a chitosan/gelatin composite film incorporated with CQDs using a hydrothermal method.[275] The inclusion of CQDs enhanced the antifungal, antibacterial, antioxidant, and UV-blocking properties of the film significantly. The composite film exhibited enhanced antibacterial efficacy, showing a ZOI of 21 ± 3 mm and 19 ± 3 mm against *L. monocytogenes* and *E. coli*, respectively. The composite film completely inhibited microbial growth after 3 hours of bacterial exposure and 24 hours of fungal exposure. Furthermore, the CQDs exhibited enhanced ROS generation, as confirmed by the oxygen radical absorbance capacity (ORAC) assay. These functional properties demonstrate the film's potential for active food packaging and smart bandage applications.

Stanković *et al.* synthesized fluorescent hydrophobic CQDs (hCQDs) using a bottom-up condensation approach.[220] They subsequently deposited uniform Langmuir–Blodgett thin films of these hCQDs on various substrates, including mica, SiO_2/Si, and glass. Compared to a pure glass sample, the hCQD films exhibited significantly enhanced antibiofouling and antibacterial activity ($R^b = 1.5$) under blue light.

4.7.2 Bioimaging. CQD-incorporated films can be promising candidates for bioimaging applications due to their intrinsic properties, including low cytotoxicity, high biocompatibility, and tunable fluorescence. Specific films, such as those fabricated from *o*-phenylenediamine-derived CQDs within a polyurethane matrix, demonstrate significant potential as bioimaging probes.[286] These composite films exhibit low cytotoxicity and high cellular uptake in HeLa cells, making them effective agents for intracellular imaging. Furthermore, structural and PL characterization of the films validated their optical properties required for high-performance, fluorescence-based imaging.

A CQD-based thin film was developed for cell labelling and imaging applications.[292] In this work, the biocompatibility and fluorescence properties of the CQDs were evaluated using the bacterial species *E. coli* and *S. aureus*, along with the fungus *A. niger*, as microbial models. The microorganisms exhibited distinct red, green, and blue fluorescence emissions after incubation, confirming successful cellular uptake of the CQDs and demonstrating their potential for microbial cell imaging.

A comprehensive summary of the key characteristics of the CQD-based films, including precursors, synthesis methods, composite matrices, fabrication techniques, and performance highlights is presented in Table 3.

5 Challenges and concerns

Although CQD-based films have shown significant promise for applications in biosensing, bioimaging, active food packaging, environmental monitoring, and membrane filtration, several critical challenges must be addressed to enable their safe, reliable, and widespread commercial adoption (Fig. 7).

5.1 Synthesis reproducibility and consistency

A major challenge in CQD synthesis is the lack of reproducibility, which hinders the scalable fabrication of consistent, uniform, and high-performance films. CQDs often display broad size distributions, variable surface chemistries, and differing impurity levels, leading to inconsistencies in critical performance metrics such as photoluminescence quantum yield, antibacterial activity, and selectivity in separation membranes.[12] Significant variations in the CQD properties, such as size and surface chemistry, may occur between batches due to subtle differences in precursor purity, reaction temperature, or reaction duration, which influence nucleation, growth, and functionalization, ultimately affecting the optical, electronic, and chemical performance of the resulting CQDs.[300,301] Aggregation and phase separation during film or membrane fabrication can further reduce effective surface area, induce fluorescence self-quenching, and introduce structural defects, compromising electronic, mechanical, and thermal properties.[7]

5.2 Scalable fabrication of high-performance films

Scaling laboratory techniques such as spin-coating, Langmuir–Blodgett deposition or drop-casting for the mass production of large-area, defect-free CQD films or membranes remain

Table 3 CQD-based composite films: precursors, synthesis, fabrication, properties, and applications

Ref.	CQD precursors	CQD synthesis process	Resultant CQDs	Polymer/ support	Fabrication method	Key features of CQDs (size, functional groups)	Performance highlights	Applications
91	Lemon extract (solvents: water and ethyl acetate)	Hydrothermal 200 °C, 5 hours	W-CQDs (W), E-CQDs (EA)	PLA	Oven drying 60 °C, 1 hour	5 ± 1 nm (W-CQDs), 2 ± 1 nm (E-CQDs), –OH, –COOH, –C═O	UV_B blocking: 82%, OTR 56%, antibacterial activity: 90%, ZOI: E-CQDs: 20 ± 3 mm (*E. coli*), 8 ± 1 mm (*S. aureus*), W-CQDs: 15 ± 2 (*E. coli*), 8 ± 1 mm (*S. aureus*)	Active food packaging
205	Dried lemon peels	Hydrothermal 200 °C, 6 hours	LCQDs	PVA	Solution casting, 25 °C, 72 hours	∼5 nm, –OH, –COOH, –C═O	TS 92.5 ± 2.1 MPa, $UV_{A,B,C}$ blocking: 99.1–99.9%, 100% antibacterial, ABTS: 98.6 ± 0.3%, DPPH: 76.5 ± 0.2	Active food packaging
206	Green tree extract	Hydrothermal 200 °C, 5 hours	CQDs	PVA	Oven drying 60 °C, 1 hour	5–35 nm, –OH, –COOH, –C═O	TS: ∼4 to ∼29 MPa, OTRs: 0.34 to 6.39 cc m^{-2} day^{-1}	Active food packaging
217	CA, EDA	Hydrothermal 200–220 °C, 5 hours	CQDs-f, CQDs-s	PVA	Piezoelectric inkjet printing	2–8 nm, –OH, –COOH, $–NH_2$, –C═O	QY: 28 ± 2% to 37 ± 2%, lifetime: 4.4 ns (CQDs-f), 6.1 ns (CQDs-s)	Anticounterfeiting
220	PE-PP-PF 68	Hydrothermal 250 °C, 2 hours	hCQDs	SiO_2/Si, glass and mica	Langmuir–Blodgett technique	∼5 nm, –OH, –COOH, –C═O	CFU mL^{-1}: 7.8 × 10^6 (*S. aureus*), 2.0 × 10^7 (*E. coli*), lifetime: 160 μs	Antimicrobial film
221	Folic acid	Hydrothermal 180 °C, 2 hours	CQDs	Dithizone-chitosan	Solvent casting	10 ± 4 nm, –OH, –COOH, –CS	Detection time: <1 min, range: 0–100 μM, limit: 18.3 nM	Pb^{2+} ion sensor
222	Folic acid	Hydrothermal 180 °C, 2 hours	CQDs	PVA	Drop casting and drying	—	QY: 32%, response time: 1 min, range: 0–100 μM, LoD: 0.006 to 0. 019 ppm	Pb, Ni, Mn, Co, and Cr detection
223	Glutathione, H_2O_2	Carbonization 250 °C, > 10 min	S-CQDs	PAH	LbL	5 nm, –OH, –COOH, –SH, $–NH_2$	Detection range: 0.10 to 5.50 μM, LoD: ∼0.05 μM, sensitivity: 241 μA cm^{-2} μmol^{-1} L^{-1}	Pb^{2+} detection
224	Phthalic acid and TED	Microwaves, 700 W, 2 min	CQDs	DPCO	Solvent casting, overnight	10 ± 2 nm, –OH, –COOH, –C═O	Fluorometric estimation LoD: 1.8 ppb (0.0068 μM), colorimetric detection LoD: 297 ppb (0.019 μM), response time: 2 min	Hg^{2+} detection
225	PA, TED	Microwaves, 850 W, 3 min	CQDs-DMG	DMG, chitosan	Solution casting	10 ± 3 nm, –OH, –COOH, $–NH_2$, –C═O	QY: 14% detection limit: 0–100 μM, LoD: 0.36 ppm (optical), 0.29 ppm, (electrochemical), response time: 1 min	Ni^{2+} detection
226	PEG-200, glucose	Microwaves, 540 W, 2 min	CQDs-CS	Chitosan	Solution casting, 60 °C, 30 min	∼1.13 nm, –OH, –COOH	Detection range: 0.1–30.0 μM, limit: 0.0112 μM	Dopamine sensor
227	PA, TED	Microwaves, 750 W, 2 min	CQDs	Chitosan	Solvent evaporation	10 ± 3 nm, –OH, –COOH, $–NH_2$, $–NO_2$	Response time: 5 min, range: 0–100 μM, limit: 0.18 ppm (EP), 0.69 ppm (MP)	EA, MP pesticide sensor
228	Laurel leaves	Hydrothermal 150 °C, 4 hours	CQDs	PPy	Solvent evaporation, 50–60 °C	∼4.5 nm, –OH, –COOH, $–NH_2$, –C═O	Zeta potential: −45.6 mV, LoD: 0.3796 mg L^{-1} sensitivity: 79.91 Hz. L mg^{-1}, detection limit: 0.58 to 5.82 ppm	Formaldehyde sensing
229	Glycerol/betaine	Hydrothermal, 180 °C, 8 hours	Gly/Bet CQDs	CMC	Drying (blast dryer)	∼8.37 nm, –OH, –COOH, –C═O	LoD: 0.452 ppm (toluene gas), detection range: 200 to 1400 mg m^{-3}, lifetime: 5.3 ns, QY: 18.34%	Hazardous (toluene) gas sensor
230	Commercial CQDs		PI, silicon	CQDs@NFCs	Spin coating, plasma etching, solvent casting		RH: 7–59%	Humidity sensors
231	*o*-PD	Hydrothermal, 200 °C, 24 hours	R-CQDs	PVA	Solvent casting	∼10 nm, red emission	Range: 190–260 K, sensitivity: 0.62% K^{-1}	Temperature sensor
232	(i) CA, DETA, PPDA	Hydrothermal 180 °C, 2–6 hours	(i) B-CQDs	PVA	Solvent evaporation	2.91, 3.01, 3.07 nm, –OH, –COOH, $–NH_2$, $–CH_2OH$	Range: 20–60 °C	Temperature sensor
	(ii) PPDA		(ii) G-CQDs					
	(iii) CA and PPDA		(iii) R-CQDs					
233	Lemon bagasse extract	Microwaves, 720 W, 5 min	CQD-L	PVA	Solvent casting, 50 °C, 48 hours	<10 nm, –OH, –COOH, –C═O	Range: 298–333 K, sensitivity: 2.69% K^{-1}, QY: 10%, IC_{50}: 276.8 ± 4.0 (O^{2-}), 21.6 ± 0.7 (HOCl)	Temperature sensor
234	CA, urea	Carbonization, 200 °C, 0.5 hours	CQDs	PVA	Solvent evaporation, 80 °C	∼1.8 nm, green emission	Range: 20–90 °C, sensitivity: 2.84% K^{-1}	Temperature sensor

Table 3 (*continued*)

Ref.	CQD precursors	CQD synthesis process	Resultant CQDs	Polymer/ support	Fabrication method	Key features of CQDs (size, functional groups)	Performance highlights	Applications
240	CA	Hydrothermal, 180 °C, 3 hours	CQDs	PI	Wet spinning and polymerization	2–6 nm, Na^+-CQDs, hollow fiber membranes	Water permeability: 47.1%, NaCl rejection: 97.7%	Brackish water desalination
241	CA, BPEI, PSS	Pyrolysis 200 °C (N_2), 2–3 hours	C-CQDs, N-CQDs, S-CQDs	PI/PSS	Interfacial polymerization	2.7–3.4 nm, –COOH, $–NH_2$, SO_3^{2-}	Flux: 42.1 L m^{-2} h^{-1}, Na_2SO_4 rejection: 93.6%	Water treatment
242	CA, glycerol, DETA	Microwaves, 750 W, 5 min	CQDs (29.6 wt%)	PEI/PAN	Interfacial polymerization	5 nm, –OH, –COOH, $–NH_2$	Flux: 42.6 L m^{-2} h^{-1} (IPA)	Organic solvent nanofiltration
243	CQDs, tertiary amine, zwitterion	Hydrothermal, 210 °C, 3 hours	CQDs, TQDs, and ZQDs	TPU, cellulose acetate	Wet phase inversion method	3.08 ± 1.32 (CQDs), 3.08 ± 1.08 (TQDs), 3.09 ± 1.10 nm (ZQDs), –OH, –COOH, $–NH_2$, $–SO^{3-}$	High flux: 6227.4 L m^{-2} h^{-1} bar^{-1} (ZQDs-M), Cu^{2+} rejection: 95.4%	Cu^{2+} detection
246	CA, EDA	Hydrothermal 150–300 °C, 5 hours	PANI/CQDs	PANI, Au/ PES	Drying, RT	3–10 nm, –OH, –COOH, $–NH_2$	Optical contrast: 53% (850 nm), retention: 95%	Electrochromic device
247	Cigarette butts, H_2SO_4	Hydrothermal 180 °C, 6 hours	N,S-CQDs (CBCDs) (9.6 wt%)	PVA	Drop casting (oven)	3.7 ± 1.4 nm, –OH, –COOH, $–NH_2$	QY: 26%, detection limit: 0.13 μM (Fe^{3+}), 0.2 μM (ascorbic acid)	Security ink, bioimaging, sensing, logic gate
248	Mango leaves	Pyrolysis, 280 °C, 3 hours	M-CQDs	ZnO nanorods	Solvent evaporation 110 °C, 1 hour	2–3 nm, –OH, –COOH, –C═O	Photocurrent density: 123.49 μA cm^{-2}, response: 0.5 nA (0 V)	UV photodetector
249	CA, urea	Hydrothermal 190 °C, 8 hours	N-CQDs/ZnO	Zn $(CH_3COO)_2$	Spin coating/tubular furnace drying 350 °C, 2 hours	∼2.5 to 3 nm, –OH, –COOH, $–NH_2$	Transparency: >95%, lifetime: 3.43 ns Higher responsivity (∼3×), external quantum efficiency (∼3×), and detectivity (∼7.5×) compared to pristine ZnO	UV photodetector
250	Acetic acid, 2-methoxyethano, cobalt acetate	Ball milling 300 rpm, 40 hours	CQD/Co_3O_4	Spinel Co_3O_4	Spin coating 350 °C, 5 min	3.2 nm, Co-doped, –OH, –COOH, –C═O	Saturation magnetization (emu cc^{-1}): 49 (IS), 95 (HRS), and 113 (LRS)	Memory device
251	Cellulose fiber, ammonia	Hydrothermal, 200 °C, 4 hours	CQDs (9 wt%)	PVA	Solvent casting 60 °C, 5 d	3–7 nm, –OH, –COOH, $–NH_2$	Shape recovery time window: 20–200 s	Water-induced shape memory
194	Graphite rods	Electrochemical 30 V, 120 hours	CQDs/PPy	SSMW	Electrochemical polymerization	–OH, –COOH, C–N	Specific capacitance: 315 mF cm^{-2} (0.2 mA cm^{-2}), cyclability: 85.7% (after 2000 cycles)	Solid state supercapacitor
196	CA, urea	Microwave 650 W, 4 min	CQDs	PET	NFDW electrospray deposition	21 ± 11 nm	Fiber radius: ∼34 ± 4.59 μm, RH: 40.1% (flow rate 0.8 mL h^{-1}, voltage 2.43 kV), fiber radius: ∼19.11 ± 4.04 μm, RH: 34% (flow rate 0.6 mL h^{-1}, voltage 2.55 kV), fiber radius: ∼29.09 ± 7.67 μm, RH: 41.1% (flow rate 0.8 mL h^{-1}) Flow rate: 0.6 to 0.8 mL h^{-1}, 3 kV	Pattern (logo, QR code fabrication)
254	Fish scale	Hydrothermal, 180 °C, 24 hours	PAPI@CQDs	PAPI	Electrospray (1 mL min^{-1}, 0–12 kV, 0–3 bar)	6 ± 1 nm, –OH, –COOH, $–NH_2$	Lifetime: 5.1–6.2 ns, specific capacity: 185.1 C g^{-1} (2 A g^{-1}), cyclability: 79.4% at 20 A g^{-1} (after 10 000 cycles)	Hybrid supercapacitor
255	CA, urea	Hydrothermal 200–250 °C, 2 hours	CQDs (70 wt%)	Cotton fabric	Vacuum heating, 80 °C, 10 min	3.34 ± 1.34 nm, –OH, –COOH, $–NH_2$, –C═O	QY: ∼79%, QY (CQDs in cotton fabrics): 42%	Anticounterfeiting
256	CA, urea	Hydrothermal, 180 °C, 5 hours	CQDs	Carbon cloth	Electrochemical deposition	∼5 nm, –OH, –COOH, $–NH_2$	Capacitance: 572.5 mF cm^{-2}, energy density: 17.04 μW h cm^{-2}, power density: 200 mW cm^{-2}	Supercapacitor
258	Na_2HPO_4, dextrose	Hydrothermal 200 °C, 1 hour	P-CQDs	PMMA/FTO-coated glass	Spin coating	3–7 nm	Photocurrent: ∼3%, fill factor: ∼6%	Solar cells
259	CA, Tris, KH-792	Hydrothermal 180 °C, 10 hours	Si-CQDs	PVA	Vacuum drying 70 °C, 1 hour	∼3.31 nm, –OH, –COOH, –C═O, $–NH_2$	QY: 86.67%, J_{sc}: 0.84 mA cm^{-2}, P_{max}: 0.201 W, power conversion: 4.76%	Photovoltaic cells

Table 3 (*continued*)

Ref.	CQD precursors	CQD synthesis process	Resultant CQDs	Polymer/ support	Fabrication method	Key features of CQDs (size, functional groups)	Performance highlights	Applications
260	a. CA/urea/$CaCl_2$ (CDs) b. EDA/H_3PO_4 (RTP-CDs)	Hydrothermal 200–250 °C, 2 hours	CQDs@PVP, CQDs@CA, CQDs@BNO	PVA Cyanic acid Boric acid	Vacuum heating 80 °C, 12 hour	5–6 nm, –OH, –COOH, $–NH_2$, –C═O	Lifetime: 9.7–12.6 ns QY: 40–67%	Anticounterfeiting
261	Lignin, EDA, formamide	Hydrothermal, 180 °C, 10 hours	F-NCQDs	PVA	Solvent evaporation, 40 °C, 24 hours	3.24, 3.42, 4.46 nm, –OH, –COOH, $–NH_2$, –C═O	QY: 42.69%	Anticounterfeiting
266	Chestnut shell and extract	Heating 100 °C, 40 min	ZnO/CQDs	ZnO, agar	Oven drying, 50 °C, 48 hours	4–6 nm, –OH, –COOH	Photocatalytic activity: >3-log CFU g^{-1}, TS: ∼15.15 MPa, OTR: 4.28 ± 0.88 cc m^{-2} day	Antimicrobial and antioxidant packages
268	HPEI and hydroxybenzaldehyde	Solvothermal 180 °C, 8 hours	D/O/M/P-CQDs	PVA	Solvent casting, 80 °C, 24 hours	1.76–4.2 nm, –OH, –COOH, –C═O, $–NH_2$	UV blocking: >98%, HEBL blocking: >85%	UV and blue light blocking
269	Lignin and EDA	Hydrothermal, 200 °C, 12 hours	N-CQDs	PVA	Solvent casting, 60 °C, 24 hours	<10 nm, –OH, –COOH, –C═O, $–NH_2$	QY: 19.61 ± 3.29%, UV blocking: 100% ($UV_{A,B,C}$), HEBL blocking: 99.9%	UV and HEBL blocking
270	CA, PEI	Hydrothermal, 180 °C, 20 hours	NH_2-CQDs	TEMPO-oxidized NC	Desiccator drying, 24 hours	–OH, –COOH, $–NH_2$	UV_A blocking: 99.8%, TS: 1.6 MPa, thermal resistance: 330 °C	Active packaging
271	CA	Oil bath, 200 °C, 2 hours	CQDs	PU	Drying 60 °C, 2 hours	5–7 nm, –OH, –COOH, –C═O, –C–N	UV resistance: >66%	UV blocking
272	Ascorbic acid, chitosan	Hydrothermal, 180 °C, 12 hours	CQDs	CMC	Solution casting, 25 °C, 48 hours	∼7.8 nm, –OH, –COOH, $–NH_2$	UV blocking: 80–100%, ABTS: 100%, DPPH: 87–88%, TS: >27.6%, EM: >61.5%	Active food packaging
273	Lemon peel	Hydrothermal, 200 °C, 3 hours	CQDs	Guar gum, SA	Solution casting, 30 °C, 48 hours	2.8 nm, –OH, –COOH, –C═O	TS: 38.80 MPa, ABTS: 43.45%, DPPH: 34.47%, ZOI: 18.94 mm (*E. coli.*), 15.45 (*S. aureus*)	Active food packaging
274	Banana peel	Hydrothermal, 180 °C, 8 hours	SCCQD	Sericin protein	Solvent casting	10 nm, –OH, –COOH	Antibacterial activity, ZOI: 146%, ∼19 mm (*B. subtilis*), 157%, ∼20 mm (*E. coli*)	Active food packaging
275	Glucose	Hydrothermal, 200 °C, 6 hours	CQDs	Chitosan, gelatin	Solvent casting, 25 °C, 48 hours	–OH, –COOH, –C═O, $–NH_2$	TS: ∼79–82 MPa, EM: ∼2.5–2.7 GPa, UV blocking: 99%, antioxidant (ABTS: 98.1%, DPPH: 74.7%,) 100% antibacterial (listeria and *E. coli.*), ZOI: 4 ± 2 (*A. flavus*), 6 ± 3 mm (*C. orbiculare*)	Active food packaging
276	Glucose	Hydrothermal, 200 °C, 6 hours	Pectin/CQDs	Pectin	Solution casting	–OH, –COOH, –C═O	100% antibacterial; ZOI (mm): 3–7 (listeria), 1–8 (*E. coli.*), 4–12 (*A. flavus*), antioxidant (ABTS: ∼95%, DPPH: ∼92%), TS: 38–43 MPa	Antibacterial and antioxidant
277	Turmeric (curcumin)	Hydrothermal, 180 °C, 12 hours	CQDs-CS	Chitosan	Solvent casting 35–40 °C, 24–48 hours	–OH, –COOH, –C═O	3.19 $\log_{10}$ CFU mL^{-1} (*S. aureus*), 2.05 CFU mL^{-1} (*E. coli*)	Active food packaging
278	Clove, PEI, cysteine	Hydrothermal, 180 °C, 8 hours	CPCDs	TPS, κ-carrageenan	Oven drying, 60 °C, 12 hours	6.5 nm, –OH, –COOH, $–NH_2$, –SH	Zeta potential: −5.85 mV, TS: >40 MPa, transparency: ∼77%, antioxidant (ABTS: >90%, DPPH: >80%)	Active food packaging
280	Grapefruit peel, zinc nitrate	Hydrothermal, 200 °C, 6 hours	Zn-GFP-CQDs	Cellulose nanofiber	Solvent casting RT, 72 hours	1–20 nm, Zn doped, –OH, –COOH, –C═O	TS: ∼59–71 MPa, UV blocking: 85.7%, antioxidant (ABTS: ∼99.81, DPPH: ∼77.44%), ZOI (mm): 24.30 ± 0.56 (*S. aureus*), 23.48 ± 0.82 mm (*S. enterica*), 17.65 ± 0.23 (*E. coli*), 17.59 ± 0.24 (*L. monocytogenes*)	Food packaging
281	CA, glycerine	Microwaves, 600 W, 15 min	CQDs	Malva extract @HNTs/ starch/HA	Solvent casting RT, 48 hours	–OH, –COOH, –C═O, $–NH_2$	TS: >266.86 MPa, ZOI: 0.4 ± 0.1 cm (*S. aureus*), 0.3 ± 0.1 cm (*E. coli*)	Antimicrobial film
282	Turmeric extract	Hydrothermal, 180 °C, 12 hours	PCH-CQDs	Chitosan/ HA/PVA	Air-dried 40 °C, 24 h	–OH, –COOH, –C═O, $–NH_2$	TS: 8.97 ± 0.93 MPa, swelling ratio: ≈250% (PBS, pH 7.4) Antibacterial activity: >2.20 (*S. aureus*), 1.28–1.45 (*E. coli*) $\log_{10}$ CFU mL^{-1}, wound closure: 69.22 ± 2.81% after 3 days	Wound dressing

Table 3 (*continued*)

Ref.	CQD precursors	CQD synthesis process	Resultant CQDs	Polymer/ support	Fabrication method	Key features of CQDs (size, functional groups)	Performance highlights	Applications
283	ATP, $LaCl_3$	Hydrothermal, 180 °C, 6 hours	La@N-P-CQDs	PVA	Drying 90 °C, 2 hours	∼2.55 nm, –NH_2, –OH, –COOH	Lifetime: 4.18 ns, antibacterial activity: >99.9% (*S. aureus* and *E. coli*), wound closure: ≥75% after 7 days	Wound dressing
285	Folic acid	Hydrothermal, 240 °C, 6 hours	CS/CQDs	Chitosan, GM L-Arginine	Solvent drying, 60 °C	1.798 nm, hydrogel film	TS: 3.43–6.60 MPa, swelling ratio: ∼800% (PBS, pH 7.4), haemostatic potential: ∼34% Blood clotting index: ∼70%, ZOI: ∼2.5 ± 0.1 cm for Gram positive and negative, cell viability: >80%	Wound dressing
287	Chitosan, $AgNO_3$	Hydrothermal, 200 °C, 12 hours	MoS_2–Ag–NCQDs	PVA	Oven drying 60 °C, 1 hour	3 ± 1 nm to 4 ± 1 nm, Ag doped, –OH, –NH_2	TS: 78.92 ± 3 MPa, OTR: 99.8%	Active food packaging
288	Banana fiber, jute, coconut husk, and water hyacinth	Hydrothermal, 200 °C, 2 hours	CQDs	PVA	Oven drying, 60 °C, 24 hours	<10 nm, –OH, –COOH, –C═O	TS: 1.05 ± 0.040 to 1.72 ± 0.002 MPa UV-blocking: 89 to 92.55%, antibacterial activity: 100% (*E. coli* and *S. aureus*)	Active food packaging
289	Crayfish shells, zinc acetate	Hydrothermal, 180 °C, 5.5 hours	Zn-CQDs	PVA	Solvent casting, 25 °C, 25 hours	2–6 nm, –OH, –COOH, Zn doped	Transmittance: 52.59–63.83% Antioxidant (ABTS: ∼94.94%, DPPH: ∼67.72%)	Active food packaging
290	Waste paper	Hydrothermal, solvothermal, 210 °C, 12 hours	D-CQD (DI) E-CQD (EtOH) P-CQD (PrOH)	PVA	Solvent evaporation, 60 °C, 1 d	2.6–4.4 nm, –OH, –COOH, –C═O	QY: 12% (D-CQDs), 27% (E-CQDs), 10% (P-CQDs)	Anticounterfeiting
291	L-Ascorbic acid, glycerol	Hydrothermal, 170 °C, 1.1 hours	ZnO/CQDs	Zinc acetate	Drying, 150 °C, 1 hour	∼5 nm, –OH, –COOH, –NH_2	LoD: 100 ppb, detection range: 100 ppb to 100 ppm, response time: 34 s, recovery time: 36 s	NO sensor
286	*o*-PD	Solvothermal, 180 °C, 12 hours	CQDs	PU	Swell-encapsulation-shrink	4 ± 1 nm, –NH_2, –OH	—	Antibacterial and bioimaging
292	CA	Flame/ combustion	CQDs	Petrol, glass/ quartz	Langmuir–Blodgett technique	0.5–1.5 nm, –OH, –COOH,	QY: 10.2%, fungal spores (*A. niger*), LoD: 0.93 μg mL^{-1}	Bioimaging
293	Dextrose, urea	Coconut oil bath, 180 °C, 24 hours	CQDs	PPy	Electrospray deposition 0–3 bar, 0 to 20 kV	∼1.5 nm, –OH, –COOH,	Capacitance: 79.25 C g^{-1} (1.5 A g^{-1}), energy density: 26.44 Wh kg^{-1}, power density: 18 090.82 W kg^{-1}, retention: 76.8% at 15 A g^{-1} (10 000 cycles)	Supercapacitor
294	L-Proline, methyl orange	Hydrothermal, 180 °C, 6 hours	N,S-CQDs	PVA	Solvent evaporation, 45 °C, 12 hours	∼5.36 nm, –COOH, –OH, –NH_2	TS: ∼27.66 MPa, detection limit: 0–25 μM, LoD: 0.94 μM, UV-blocking: 99.5%, QY: 22.5% (ethanol) & 12.7% (acetone), lifetime: 6.73 ns	Active food packaging and chlortetracycline (CTC) detection
295	Banana leaf	Hydrothermal, 200 °C, 15 hours	CQDs	PVP/glass	Spin coating, (400 rpm, 40 s), vacuum drying, 30 °C, 12 hours	∼3.48 nm, –C═O, –OH, –NH_2	EQE: 15.25%, PCE: 15.94%, V_{oc}: 6.77 V, J_{sc}: 3.19 mA cm^{-2}, FF: 73.6% at 0.4% CQDs	Solar cells
296	Damask rose	Hydrothermal, 190 °C, 24 hours	CQDs	PDA	Drop-cast on Al foil, oven dry @ 50 °C	∼3.3 nm, –OH, –COOH,	Detection range: 0.1 to 345 μM, LoD: 0.069 μM in 0.1 M PBS, zeta potential: −19 mV	Dopamine detection (amperometry)
297	Stinging nettle (herbal tea)	Hydrothermal, 200 °C, 7 hours	CQDs	CNF	Solvent evaporation, 25 °C	3.4 ± 0.52 nm, –OH, –COOH, –C═O	TS: 59.7 ± 2.1 MPa, UV blocking: 85.2% (UV_A), 58.9% (UV_B), ZOI: *S. enterica* (86.4 ± 1.7%), *S. aureus* (97.1 ± 1.1%), *E. coli* (72.2 ± 2.0%), *L. monocytogenes* (94.9 ± 1.6%), ABTS: 100.0%	Active packaging

Table 3 (*continued*)

Ref.	CQD precursors	CQD synthesis process	Resultant CQDs	Polymer/ support	Fabrication method	Key features of CQDs (size, functional groups)	Performance highlights	Applications
298	Neem leaves	Hydrothermal, 180 °C, 6 hours	N-CQDs	Ethyl cellulose/PEO	Electrospray deposition flow rate: 1.2 mL h^{-1}, 18 kV	~2.57 nm, –COOH, –C═O, –OH, $–NH_2$,	TS: ~2.65–7.22 MPa, UV_A: 99.92% and UV_B: 99.98% blocking, ABTS: ~90%, DPPH: ~73%, zeta potential: –12.78 mV, QY: ~3.65%	Active packaging
299	*o*-PD, 3,4-DBSA	Hydrothermal, 200 °C, 12 hours	CQDs-(1–3)	PLA, HFPI	Electrospray deposition, flow rate: 1–1.5 mL h^{-1}, 18 kV	4.93 ± 1.44, 3.08 ± 1.02, 1.96 ± 0.73 nm, –OH, –COOH, –C═O, –OH, $–NH_2$	TS: 2.78 ± 0.24, 2.91 ± 0.11, 3.78 ± 0.2 MPa, zeta potential: –34.1, +16.9, –23.3 mV, ABTS: 77.9 ± 0.2, 90.76 ± 1.0, 96.95 ± 0.3%, DPPH: 69.73 ± 1.16%, 75.8 ± 1.27%, and 79.16 ± 0.09%, RH: 80%	Active packaging

3,4-DBSA: 3,4-diaminobenzene sulfonic acid, ABTS: 2,2′-azino-bis(3-ethylbenzothiazoline-6-sulfonic acid), ASSS: all-solid-state supercapacitors, ATP: adenosine triphosphate, BPEI: branched polyethyleneimine, CA: citric acid, CMC: carboxymethyl cellulose, CNF: cellulose nanofiber, CPCDs: clove, polyethylenimine and cysteine derived CQDs, CQDs-f: CQDs with fast fluorescence lifetimes, CQDs-s: CQDs with slow fluorescence lifetimes, CTC: chlortetracycline, D-CQDs: 2,4-dihydroxybenzaldehyde CQDs, DETA: diethylenetriamine, DMG: dimethylglyoxime, DPCO: 1,5-diphenylcarbazone, DPPH: 2,2-diphenyl-1-picrylhydrazyl, E-CQDs (EA): lemon extract-dispersed CQDs (ethyl acetate), EM: elastic modulus, EP: ethyl paraoxon, EQE: external quantum efficiency, FA: folic acid, F-NCQDs: N-doped lignin-based CDs in formamide, HFPI: hexafluoroisopropanol, HNT: halloysite nanotubes, hCQDs: hydrophobic carbon dots, KH-792: *N*-[3-(trimethoxysilyl)propyl]ethylenediamine, M-CQDs: *m*-hydroxybenzaldehyde CQDs, MP: methyl parathion, NFC: nanofiber clusters, NFDW: near-field direct write, O-CQDs: *o*-hydroxybenzaldehyde CQDs, *o*-PD: *o*-phenylenediamine, OTR: oxygen transmission rate, P-CQDs: *p*-hydroxybenzaldehyde CQDs, PA: phthalic acid, PAH: poly(allylamine hydrochloride), PAN: polyacrylonitrile, PAPI: poly(aniline-*co*-indole), PD: photodetector, PDA: polydopamine, PE–PP–PF 68: polyoxyethylene–polyoxypropylene–polyoxyethylene Pluronic 68, PEG: polyethylene glycol, PEO: poly(ethylene oxide), PES: polyethersulfone, PLA: polylactic acid, PMMA: poly(methyl methacrylate), PPy: polypyrrole, PSS: poly(sodium 4-styrene sulfonate), PVA: polyvinyl alcohol, SA: sodium alginate, SCCQD: sericin protein CQD, SSMW: stainless steel wire meshes, TED: triethylene diamine, TPS: thermoplastic starch, TPU: thermoplastic polyurethane, tris: tris(hydroxymethyl)aminomethane, TS: tensile strength, W-CQDs (W): lemon extract-dispersed CQDs (water solvent).

challenging. Achieving uniform thickness, controlled porosity, and homogeneous CQD distribution, along with robust integration with host matrices such as polymers and metals, is difficult due to poor interfacial compatibility arising from mismatched surface energies and polarities. Chemical interactions between CQD surface functional groups and the polymer matrix can induce defects and crosslinking, promoting non-radiative energy transfer and thereby quenching PL.[302] Additionally, CQD aggregation can lead to uneven dispersion, further reducing functional performance. These limitations further complicate the scalability of CQD-based films for industrial applications. Therefore, further research into scalable and controllable deposition techniques, such as spray coating, roll-to-roll fabrication, and slot-die coating, is needed, as these methods can produce large-area, uniform films while mitigating issues such as aggregation, uneven thickness, and poor integration with polymer substrates.[300,301,303]

5.3 Performance and long-term stability

CQD-based films and membranes are susceptible to degradation caused by photobleaching, oxidative damage, and harsh conditions such as high salinity or varying humidity, pH, and temperature.[107,304] In addition, limited structural control, heterogeneous surface defects, and nanoparticle aggregation broaden the emission bandwidth of many CQDs, compromising color purity and reducing quantum yield, particularly in the near-infrared region.[305,306] Additionally, the high surface-to-volume ratio and diverse surface ligands can also lead to inconsistent functional properties, negatively affecting the reproducibility, uniformity, and long-term stability of the films in practical applications.[307]

5.4 Safety, toxicity, and environmental concerns

Carbon quantum dots are generally nontoxic and more biocompatible than conventional heavy metal-based quantum dots. However, CQD films can undergo leaching during application or disposal, particularly under mechanical or environmental stress or in the presence of solvents, releasing surface ligands, CQD fragments, or adsorbed contaminants into the surrounding medium and posing potential risks to human health and the environment. The high surface-to-volume ratio of CQD films further increases the likelihood of adsorption and transport of external agents. Toxicity may arise from residual precursors and catalysts and can be influenced by surface functional groups, metal incorporation, heteroatom dopants, particle size, surface charge, and oxidative or photolytic degradation.[13,14,308] Exposure to high concentrations of CQDs can induce cytotoxicity, oxidative stress, and inflammatory responses in mammalian cells.[14] CQDs can also affect aquatic organisms, including phytoplankton, zooplankton, and benthic species, raising concerns about environmental accumulation and long-term ecological impacts.[15] Neurological effects, including neuronal damage, have been reported under enhanced exposure or inhalation.[309] These risks may be aggravated during large-scale production, particularly if residual contaminants or dopants are present. However, the

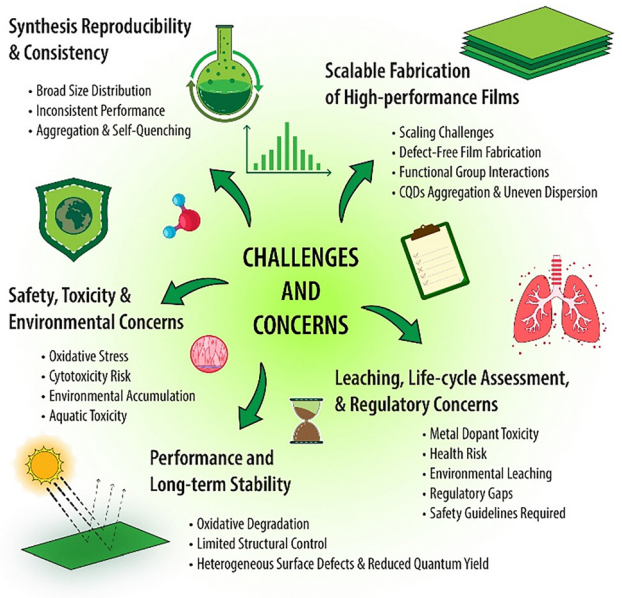

Fig. 7 Challenges in CQD-based film development and applications.

toxicological implications of CQD-incorporated polymers remain insufficiently studied for safety-critical applications such as food packaging and biomedical devices. Comprehensive assessment of these effects is essential for the sustainable and safe use of CQD-based materials.

5.5 Life-cycle assessment

Life-cycle assessment (LCA) provides a systematic framework to evaluate the environmental and safety impacts of CQD films from synthesis to disposal. Factors such as fabrication methods, precursor types, energy consumption, and waste generation critically influence sustainability metrics, including carbon footprint, water use, and chemical hazard potential. However, the absence of comprehensive LCA studies leaves the overall environmental footprint of these films uncertain.[310,311]

Green synthesis approaches,[312] including biomass-derived precursors, as well as ecofriendly solvent-free methods (*e.g.*, solid-state or mechanochemical synthesis) and low-energy approaches (*e.g.*, hydrothermal or microwave-assisted synthesis),[311] can reduce toxic residues, minimize solvent waste, lower energy consumption per unit of film. Additionally, scalable deposition techniques like spray coating, roll-to-roll fabrication, and slot-die coating enable the production of large-area films with uniform thickness and controlled morphology, reducing material waste and defects while enhancing overall energy and resource efficiency. Incorporating these strategies within an LCA framework can provide quantitative insights into environmental trade-offs and guide the sustainable development of CQD-based films.

5.6 Regulatory considerations

Despite increasing interest in CQD-based films, the regulatory framework specific to their use remains limited. Existing frameworks from agencies such as the US FDA, EU, and OECD provide general protocols for toxicity, safety, and environmental assessment,[313,314] but do not fully address the unique physicochemical properties of CQDs, including nanoscale size, surface functionalization, and potential leaching. The limited availability of systematic data on toxicity, migration, bioaccumulation, and long-term exposure further complicates regulatory approval, particularly for applications in healthcare, food preservation, and environmental systems.

In addition, the lack of standardized characterization and testing protocols remains a critical challenge. While techniques such as TEM, SEM, FTIR, XRD, and XPS are widely used,[315] inconsistencies in sample preparation, measurement conditions, and data interpretation hinder reliable comparison across studies. The development of harmonized safety evaluation protocols, standardized testing methods, and clear regulatory guidelines for production, use, and disposal is critical for enabling reliable risk assessment and ensuring the safe deployment of CQD-based materials. These measures will facilitate their translation from laboratory research to commercial applications while minimizing potential ecological and health risks.[303]

Addressing these interrelated challenges is essential for translating CQD-based materials from promising laboratory studies to reliable, safe, and sustainable commercial applications.

6 Conclusions

Carbon quantum dots are a cost-effective and highly versatile class of nanomaterials, characterized by their quantum-confined PL, tunable optoelectronic properties, and rich surface chemistry. They can be synthesized efficiently using various top-down and bottom-up methods from a wide range of natural and biomass-derived precursors, enabling sustainable and cost-effective large-scale production of CQDs. These advanced synthesis approaches also allow precise control over particle size, heteroatom doping, and surface functionalization.

These nanomaterials can be incorporated into a wide range of polymer matrices and inorganic substrates, allowing for the fabrication of multifunctional and application-specific composite materials. Advanced thin-film deposition techniques, including electrospinning, solvent casting, Langmuir–Blodgett deposition, inkjet printing, and spray coating, enable the fabrication of functional thin films with precisely tailored properties for applications such as fluorescence sensing, UV shielding, catalytic degradation, anti-counterfeiting, antimicrobial activity, and flexible optoelectronics. Moreover, their carbon-based composition provides low toxicity and excellent biocompatibility, making CQD-based films promising materials for biomedical, environmental, and sustainable packaging applications.

However, several key challenges must be addressed to enable the widespread adoption of CQD-based films in commercial applications. The lack of reproducible and

standardized synthesis protocols may cause variations in particle size, composition, and surface chemistry, thus affecting the consistency and performance of the resulting films. Additionally, nanoparticle aggregation and surface non-uniformities remain major obstacles to fabricating large-area, defect-free thin films, making scalable manufacturing difficult. Besides, achieving long-term reliability and environmental stability of CQD-based films under operational stresses, including prolonged light exposure and fluctuations in temperature, pH, and humidity, remains a significant challenge. Furthermore, potential ecological risks of CQD-based films, including their toxicity and bioaccumulation, must be thoroughly studied to ensure the safe and sustainable use of these materials.

In addition to addressing these challenges, future research should be directed towards the development of advanced CQD composites and their integration into functional devices. Integrating CQDs with complementary nanomaterials, such as two-dimensional semiconductors or metal–organic frameworks, can potentially result in synergistic improvements in charge transport, catalytic activity, optical performance, and mechanical robustness. Additionally, continued efforts are required to translate these materials into functional next-generation devices, including field-effect transistors, wearable optoelectronic sensors, artificial synapses for neuromorphic computing, and sustainable energy storage and conversion systems.

By addressing existing challenges and through continued research and innovation, CQD-based films can evolve into a versatile and sustainable materials platform with strong potential for multifaceted applications in flexible and wearable healthcare devices, optoelectronics, food preservation and packaging, filtration systems, and diverse environmental remediation technologies.

Author contributions

Arup Kumer Roy and Sumit Majumder contributed to the conceptualization and methodology. Arup Kumer Roy, Ayesha Binth Humayun, Yuv-raj Acharjee, and Nusrat Jahan Usha performed the investigation and data curation, with Arup Kumer Roy leading the formal analysis and visualization. The original draft was prepared by Arup Kumer Roy and Ayesha Binth Humayun, and Sumit Majumder provided review, editing, and supervision.

Conflicts of interest

There are no conflicts to declare.

Data availability

No primary research results, software or code have been included and no new data were generated or analysed as part of this review.

Acknowledgements

This work was supported by the Directorate of Research and Extension (DRE) at Chittagong University of Engineering and Technology under project code CUET/DRE/2025-2026/BME/001.

References

1 Y. Wang and A. Hu, *J. Mater. Chem. C*, 2014, **2**, 6921–6939, DOI: 10.1039/c4tc00988f.
2 P. Kumar, S. Dua, R. Kaur, M. Kumar and G. Bhatt, *RSC Adv.*, 2022, **12**, 4714–4759, DOI: 10.1039/d1ra08452f.
3 Y. Deng, M. Chen, G. Chen, W. Zou, Y. Zhao, H. Zhang and Q. Zhao, *ACS Omega*, 2021, **6**, 4247–4254, DOI: 10.1021/acsomega.0c05182.
4 H. Shabbir, E. Csapó and M. Wojnicki, *Inorganics*, 2023, **11**, 262, DOI: 10.3390/inorganics11060262.
5 F. Li, D. Yang and H. Xu, *Chem. – Eur. J.*, 2019, **25**, 1165–1176, DOI: 10.1002/chem.201802793.
6 J. Kong, Y. Wei, F. Zhou, L. Shi, S. Zhao, M. Wan and X. Zhang, *Molecules*, 2024, **29**, 2002, DOI: 10.3390/molecules29092002.
7 A. Kamal, S. Hong and H. Ju, *Biosensors*, 2025, **15**, 99, DOI: 10.3390/bios15020099.
8 A. Piasek and J. Pulit-Prociak, *Nanoscale*, 2025, 1–9, DOI: 10.1039/d5nr02878g.
9 M. Tavan, Z. Yousefian, Z. Bakhtiar, M. Rahmandoust and M. H. Mirjalili, *Ind. Crops Prod.*, 2025, **231**, 121207, DOI: 10.1016/j.indcrop.2025.121207.
10 A. K. Singh, P. Itkor, M. Lee, A. Saenjaiban and Y. S. Lee, *Molecules*, 2024, **29**, 5138, DOI: 10.3390/molecules29215138.
11 M. Mujahid, *Adv. Nat. Sci. Nanosci. Nanotechnol.*, 2025, **16**, 033001, DOI: 10.1088/2043-6262/addcdd.
12 I. Eliboev, A. Ishankulov, E. Berdimurodov, K. Chulpanov, M. Nazarov, B. Jamshid, B. Toshpulotov, R. Tukhtaeva, M. Demir, K. Rashidova, F. Jalilov and K. Polvonov, *Anal. Methods*, 2025, **17**, 2627–2649, DOI: 10.1039/d4ay02237h.
13 Y. Y. Liu, N. Y. Yu, W. D. Fang, Q. G. Tan, R. Ji, L. Y. Yang, S. Wei, X. W. Zhang and A. J. Miao, *Nat. Commun.*, 2021, **12**, 812, DOI: 10.1038/s41467-021-21080-z.
14 J. Mishra, T. Suryawanshi, N. Redkar, R. K. Das, S. Saxena, A. Majumder, K. Kondabagil and S. Shukla, *ChemSusChem*, 2025, **18**, e202402056, DOI: 10.1002/cssc.202402056.
15 X. Li, C. C. Chen, L. Wu, J. Zhou, Y. Huang and X. Zhu, *Mar. Pollut. Bull.*, 2024, **199**, 115921, DOI: 10.1016/j.marpolbul.2023.115921.
16 D. H. H. Nguyen, H. El-Ramady and J. Prokisch, *Environ. Chem. Lett.*, 2025, **23**, 337–360, DOI: 10.1007/s10311-024-01779-3.
17 J. Tan and L. Zhou, *Ind. Crops Prod.*, 2024, **210**, 118086, DOI: 10.1016/j.indcrop.2024.118086.
18 A. Tyagi, K. M. Tripathi, N. Singh, S. Choudhary and R. K. Gupta, *RSC Adv.*, 2016, **6**, 72423–72432, DOI: 10.1039/c6ra10488f.

19 X. Hu, Y. Li, Y. Xu, Z. Gan, X. Zou, J. Shi, X. Huang, Z. Li and Y. Li, *Food Chem.*, 2021, **339**, 127775, DOI: 10.1016/j.foodchem.2020.127775.
20 T. H. Huang, Y. C. Chen, W. C. Wang, Y. T. Yen, Y. P. Tsai and C. H. Lin, *J. Photochem. Photobiol., A*, 2025, **469**, 116603, DOI: 10.1016/j.jphotochem.2025.116603.
21 S. Akula, P. Varathan, R. S. Menon and A. K. Sahu, *Sustainable Energy Fuels*, 2021, **5**, 886–899, DOI: 10.1039/d0se01214a.
22 N. S. Kunnath Parambil, A. Dasan, A. T. Premkumar, N. K. Renuka and S. J. Raphael, *Sens. Int.*, 2025, **6**, 100301, DOI: 10.1016/j.sintl.2024.100301.
23 L. Han, Y. Guo, H. Zhang, Z. Wang, F. Zhang, Y. Wang, X. Li, Y. Wang and J. Ye, *RSC Adv.*, 2024, **14**, 1813–1821, DOI: 10.1039/d3ra06799h.
24 W. Lu, X. Qin, S. Liu, G. Chang, Y. Zhang, Y. Luo, A. M. Asiri, A. O. Al-Youbi and X. Sun, *Anal. Chem.*, 2012, **84**, 5351–5357, DOI: 10.1021/ac3007939.
25 J. Zhou, Z. Sheng, H. Han, M. Zou and C. Li, *Mater. Lett.*, 2012, **66**, 222–224, DOI: 10.1016/j.matlet.2011.08.081.
26 Y. A. Saber, M. Hamed, S. Emara, F. R. Mansour, M. Locatelli and N. Ibrahim, *Heliyon*, 2024, **10**, e40661, DOI: 10.1016/j.heliyon.2024.e40661.
27 H. Salimi Shahraki, Qurtulen and A. Ahmad, *Inorg. Chem. Commun.*, 2023, **150**, 110514, DOI: 10.1016/j.inoche.2023.110514.
28 C. Cheng, Y. Shi, M. Li, M. Xing and Q. Wu, *Mater. Sci. Eng., C*, 2017, **79**, 473–480, DOI: 10.1016/j.msec.2017.05.094.
29 M. S. Devi, T. D. Thangadurai, N. Manjubaashini and D. Nataraj, *Diamond Relat. Mater.*, 2023, **136**, 110021, DOI: 10.1016/j.diamond.2023.110021.
30 J. Zhu, F. Zhu, X. Yue, P. Chen, Y. Sun, L. Zhang, D. Mu and F. Ke, *J. Nanomater.*, 2019, **2019**, 7965756, DOI: 10.1155/2019/7965756.
31 N. Manjubaashini, P. Bargavi and S. Balakumar, *J. Photochem. Photobiol., A*, 2024, **454**, 115702, DOI: 10.1016/j.jphotochem.2024.115702.
32 S. Jayaweera, K. Yin, X. Hu and W. J. Ng, *J. Photochem. Photobiol., A*, 2019, **370**, 156–163, DOI: 10.1016/j.jphotochem.2018.10.052.
33 G. Gedda, C. Y. Lee, Y. C. Lin and H. F. Wu, *Sens. Actuators, B*, 2016, **224**, 396–403, DOI: 10.1016/j.snb.2015.09.065.
34 D. Elango, J. S. Packialakshmi, V. Manikandan and P. Jayanthi, *Mater. Lett.*, 2022, **312**, 131667, DOI: 10.1016/j.matlet.2022.131667.
35 D. Elango, J. Saranya Packialakshmi, V. Manikandan and P. Jayanthi, *Mater. Lett.*, 2022, **313**, 131822, DOI: 10.1016/j.matlet.2022.131822.
36 R. Bandi, B. R. Gangapuram, R. Dadigala, R. Eslavath, S. S. Singh and V. Guttena, *RSC Adv.*, 2016, **6**, 28633–28639, DOI: 10.1039/c6ra01669c.
37 A. Piasek, M. Zielina, M. Banach and J. Pulit-Prociak, *Diamond Relat. Mater.*, 2025, **156**, 112421, DOI: 10.1016/j.diamond.2025.112421.
38 D. Jessy Mercy, V. Kiran, A. Thirumalai, K. Harini, K. Girigoswami and A. Girigoswami, *Results Chem.*, 2023, **6**, 101219, DOI: 10.1016/j.rechem.2023.101219.
39 S. K. Rajkishore, K. P. Devadharshini, P. Sathya Moorthy, V. S. Reddy Kiran Kalyan, R. Sunitha, M. Prasanthrajan, M. Maheswari, K. S. Subramanian, N. Sakthivel and R. Sakrabani, *Sustainability*, 2023, **15**, 10924, DOI: 10.3390/su151410924.
40 G. Huang, X. Chen, C. Wang, H. Zheng, Z. Huang, D. Chen and H. Xie, *RSC Adv.*, 2017, **7**, 47840–47847, DOI: 10.1039/c7ra09002a.
41 S. Pandiyan, L. Arumugam, S. P. Srirengan, R. Pitchan, P. Sevugan, K. Kannan, G. Pitchan, T. A. Hegde and V. Gandhirajan, *ACS Omega*, 2020, **5**, 30363–30372, DOI: 10.1021/acsomega.0c03290.
42 M. Hamed, I. Ibrahim, A. Bedair, F. R. Mansour, S. Emara and W. Zarad, *Talanta Open*, 2025, **12**, 100492, DOI: 10.1016/j.talo.2025.100492.
43 J. Shi, Y. Zhou, J. Ning, G. Hu, Q. Zhang, Y. Hou and Y. Zhou, *Spectrochim. Acta, Part A*, 2022, **281**, 121597, DOI: 10.1016/j.saa.2022.121597.
44 L. Zhu, H. Wu, H. Yang, D. Shen, H. Hu and M. Dou, *Bioresour. Technol.*, 2024, **413**, 131490, DOI: 10.1016/j.biortech.2024.131490.
45 X. Yin, Z. Zhang, F. Li, M. Fu, T. Qin, X. Ji, Y. Wang, Z. Wang and S. Sun, *Exploration*, 2025, **5**, 20230039, DOI: 10.1002/EXP.70039.
46 X. Qin, W. Lu, A. M. Asiri, A. O. Al-Youbi and X. Sun, *Catal. Sci. Technol.*, 2013, **3**, 1027–1035, DOI: 10.1039/c2cy20635h.
47 E. A. Diab, M. Ghali and M. M. Mosaad, *Sci. Rep.*, 2025, **15**, 2212, DOI: 10.1038/s41598-025-99841-9.
48 Y. Liu, Y. Zhao and Y. Zhang, *Sens. Actuators, B*, 2014, **196**, 647–652, DOI: 10.1016/j.snb.2014.02.053.
49 Y. Qu, L. Yu, B. Zhu, F. Chai and Z. Su, *New J. Chem*, 2020, **44**, 1500–1507, DOI: 10.1039/c9nj05285b.
50 A. Sachdev and P. Gopinath, *Analyst*, 2015, **140**, 4260–4269, DOI: 10.1039/c5an00454c.
51 R. Hesham, H. Abd El-Aziz and R. El-Shaheny, *Microchem. J.*, 2025, **208**, 112322, DOI: 10.1016/j.microc.2024.112322.
52 Q. Zhang, X. Zhang, L. Bao, Y. Wu, L. Jiang, Y. Zheng, Y. Wang and Y. Chen, *J. Anal. Methods Chem.*, 2019, **2019**, 8183134, DOI: 10.1155/2019/8183134.
53 R. Kampangta, A. Saenchoopa, W. Obrom, W. S. T. Tun, C. Muanprasat, K. Maeda, P. Suwannapaporn, C. Suppaso, W. Seemakram, S. Boonlue and S. Kulchat, *Nanoscale Adv.*, 2025, **7**, 6646–6658, DOI: 10.1039/d5na00264h.
54 M. M. Ayad, M. E. Abdelghafar, N. L. Torad, Y. Yamauchi and W. A. Amer, *Chemosphere*, 2023, **312**, 137031, DOI: 10.1016/j.chemosphere.2022.137031.
55 J. Singh, S. Kaur, J. Lee, A. Mehta, S. Kumar, K. H. Kim, S. Basu and M. Rawat, *Sci. Total Environ.*, 2020, **720**, 137604, DOI: 10.1016/j.scitotenv.2020.137604.
56 G. Chellasamy, S. K. Arumugasamy, S. Govindaraju and K. Yun, *Chemosphere*, 2022, **287**, 131915, DOI: 10.1016/j.chemosphere.2021.131915.
57 P. K. Yadav, V. K. Singh, S. Chandra, D. Bano, V. Kumar, M. Talat and S. H. Hasan, *ACS Biomater. Sci. Eng.*, 2019, **5**, 623–632, DOI: 10.1021/acsbiomaterials.8b01528.

58 H. Ren, Y. Yuan, A. Labidi, Q. Dong, K. Zhang, E. Lichtfouse, A. A. Allam, J. S. Ajarem and C. Wang, *Chin. Chem. Lett.*, 2023, **34**, 107998, DOI: 10.1016/j.cclet.2022.107998.
59 W. A. Amer, A. F. Rehab, M. E. Abdelghafar, N. L. Torad, A. S. Atlam and M. M. Ayad, *Carbon*, 2021, **179**, 159–171, DOI: 10.1016/j.carbon.2021.03.047.
60 K. Shivaji, S. Mani, P. Ponmurugan, C. S. De Castro, M. Lloyd Davies, M. G. Balasubramanian and S. Pitchaimuthu, *ACS Appl. Nano Mater*, 2018, **1**, 1683–1693, DOI: 10.1021/acsanm.8b00147.
61 A. K. Roy, W. Ghann, S. Rabi, J. Barua, S. Majumder, R. Amin, M. K. M. Ziaul Hyder and J. Uddin, *RSC Sustainable*, 2024, **2**, 1003–1013, DOI: 10.1039/d3su00452j.
62 C. Zhou, J. Du, H. Zhao, Z. Xiong and L. Zhao, *J. Mol. Struct.*, 2023, **1278**, 134959, DOI: 10.1016/j.molstruc.2023.134959.
63 K. Doshi and A. A. Mungray, *J. Environ. Chem. Eng.*, 2020, **8**, 104174, DOI: 10.1016/j.jece.2020.104174.
64 S. Elkun, M. Ghali, T. Sharshar and M. M. Mosaad, *Sci. Rep.*, 2024, **14**, 27927, DOI: 10.1038/s41598-024-78745-0.
65 N. Murugan, M. Prakash, M. Jayakumar, A. Sundaramurthy and A. K. Sundramoorthy, *Appl. Surf. Sci.*, 2019, **476**, 468–480, DOI: 10.1016/j.apsusc.2019.01.090.
66 K. M. Tripathi, T. S. Tran, T. T. Tung, D. Losic and T. Kim, *J. Nanomater.*, 2017, **2017**, 7029731, DOI: 10.1155/2017/7029731.
67 A. Dager, T. Uchida, T. Maekawa and M. Tachibana, *Sci. Rep.*, 2019, **9**, 14004, DOI: 10.1038/s41598-019-50397-5.
68 S. Marouzi, M. Darroudi, A. Hekmat, K. Sadri and R. Kazemi Oskuee, *J. Environ. Chem. Eng.*, 2021, **9**, 105461, DOI: 10.1016/j.jece.2021.105461.
69 M. Puchaicela, D. Lara, V. J. Cevallos, A. Garzón, J. Gardener, G. Solorzano, L. Spencer and J. Chimborazo, *Carbon Trends*, 2025, **20**, 100493, DOI: 10.1016/j.cartre.2025.100493.
70 A. Dager, A. Baliyan, S. Kurosu, T. Maekawa and M. Tachibana, *Sci. Rep.*, 2020, **10**, 12333, DOI: 10.1038/s41598-020-69264-9.
71 A. Kumar and A. K. Gathania, *Spectrochim. Acta, Part A*, 2026, **348**, 127142, DOI: 10.1016/j.saa.2025.127142.
72 M. Xue, M. Zou, J. Zhao, Z. Zhan and S. Zhao, *J. Mater. Chem. B*, 2015, **3**, 6783–6789, DOI: 10.1039/c5tb01073j.
73 N. G. Alamdari, H. Almasi, M. Moradi and M. Akhgari, *Waste Biomass Valorization*, 2023, **14**, 3689–3703, DOI: 10.1007/s12649-023-02087-7.
74 S. Zhao, M. Lan, X. Zhu, H. Xue, T. W. Ng, X. Meng, C. S. Lee, P. Wang and W. Zhang, *ACS Appl. Mater. Interfaces*, 2015, **7**, 17054–17060, DOI: 10.1021/acsami.5b03228.
75 D. Ghosh Dastidar, P. Mukherjee, D. Ghosh and D. Banerjee, *Colloids Surf., A*, 2021, **611**, 125781, DOI: 10.1016/j.colsurfa.2020.125781.
76 R. V. Murugan, G. Sridharan, R. Atchudan, S. Arya, D. Ganapathy and A. K. Sundramoorthy, *Curr. Nanosci.*, 2024, **21**, 521–531, DOI: 10.2174/0115734137300899240509100717.
77 Y. Feng, D. Zhong, H. Miao and X. Yang, *Talanta*, 2015, **140**, 128–133, DOI: 10.1016/j.talanta.2015.03.038.
78 O. G. Rojas-Valencia, M. Regules-Carrasco, J. Hernández-Fuentes, C. M. R. S. Germán, M. Estrada-Flores and E. Villagarcía-Chávez, *Materialia*, 2021, **19**, 101182, DOI: 10.1016/j.mtla.2021.101182.
79 Q. Liu, W. Li, X. Qiao and H. Zhao, *Ind. Crops Prod.*, 2024, **213**, 118416, DOI: 10.1016/j.indcrop.2024.118416.
80 D. Soren, J. Panda, J. Swain, A. Priyadarshini, S. Swain, J. Swain, R. Pati, S. R. Mohapatra, Y. Das, R. Samantaray and R. Sahu, *Sci. Rep.*, 2025, **15**, 33727, DOI: 10.1038/s41598-025-87341-9.
81 N. Yadav, D. Mudgal, A. Mishra, S. Shukla, T. Malik and V. Mishra, *PLoS One*, 2024, **19**, e0296270, DOI: 10.1371/journal.pone.0296270.
82 A. Kumar, P. K. Gupta, M. Srivastava, A. Pandey, A. Srivastava and S. K. Srivastava, *IEEE Sens. J.*, 2022, **22**, 21635–21641, DOI: 10.1109/JSEN.2022.3211846.
83 R. Atchudan, T. N. J. I. Edison, M. G. Sethuraman and Y. R. Lee, *Appl. Surf. Sci.*, 2016, **384**, 432–441, DOI: 10.1016/j.apsusc.2016.05.054.
84 A. Başoğlu, *Luminescence*, 2025, **40**, e70099, DOI: 10.1002/bio.70099.
85 Q. Zhang, J. Liang, L. Zhao, Y. Wang, Y. Zheng, Y. Wu and L. Jiang, *Front. Chem.*, 2020, **8**, 665, DOI: 10.3389/fchem.2020.00665.
86 N. Sharma, I. Sharma and M. K. Bera, *J. Fluoresc.*, 2022, **32**, 1039–1049, DOI: 10.1007/s10895-022-02923-4.
87 P. Huang, S. Xu, M. Zhang, W. Zhong, Z. Xiao and Y. Luo, *Phys. Chem. Chem. Phys.*, 2019, **21**, 26133–26145, DOI: 10.1039/c9cp04880d.
88 X. Li, Y. Lu, J. Li, S. Zhou, Y. Wang, L. Li and F. Zhao, *J. Nanobiotechnol.*, 2022, **20**, 236, DOI: 10.1186/s12951-022-01498-3.
89 Z. Lai, X. Guo, C. Cheng, G. Ruan and F. Du, *ChemistrySelect*, 2020, **5**, 1956–1960, DOI: 10.1002/slct.201904517.
90 S. I. Alaqel, O. Abdullah, A. Alharbi, Y. S. Althobaiti, M. S. Alturki, S. Ramzy and A. H. Almalki, *RSC Adv.*, 2023, **13**, 17765–17774, DOI: 10.1039/d3ra02855k.
91 S. Han, J. R. Ansari, K. Park, K. Sadeghi and J. Seo, *J. Ind. Eng. Chem.*, 2026, **153**, 395–408, DOI: 10.1016/j.jiec.2025.05.059.
92 A. Kundu, B. Maity and S. Basu, *ACS Omega*, 2023, **8**, 22178–22189, DOI: 10.1021/acsomega.3c02474.
93 N. A. Mahat and S. A. Shamsudin, *IOP Conf. Ser.: Mater. Sci. Eng.*, 2020, **736**, 052001, DOI: 10.1088/1757-899X/736/5/052001.
94 R. Atchudan, T. N. J. I. Edison and Y. R. Lee, *J. Colloid Interface Sci.*, 2016, **482**, 8–18, DOI: 10.1016/j.jcis.2016.07.058.
95 M. Lu, Y. Duan, Y. Song, J. Tan and L. Zhou, *J. Mol. Liq.*, 2018, **269**, 766–774, DOI: 10.1016/j.molliq.2018.08.101.
96 S. Viji, A. Dinesh, K. Radhakrishnan, L. S. Priya, C. Sivasankari, M. Santhamoorthy, M. Ayyar, V. Mohanavel, M. Hashem, H. Fouad, G. Ramachandran and S. Santhoshkumar, *Sens. Bio-Sensing Res.*, 2025, **47**, 100756, DOI: 10.1016/j.sbsr.2025.100756.
97 K. Kasirajan, M. Karunakaran and H. K. Choi, *J. Environ. Chem. Eng.*, 2024, **12**, 113535, DOI: 10.1016/j.jece.2024.113535.

98 C. Salih Ajaj and D. Sadiq, *Nanomater. Nanotechnol.*, 2023, **2023**, 9980479, DOI: 10.1155/2023/9980479.
99 K. S. Rawat, V. Singh, C. P. Sharma, A. Vyas, P. Pandey, J. Singh, N. M. Gupta, M. Sachdev and A. Goel, *J. Imaging*, 2023, **9**, 19, DOI: 10.3390/jimaging9010019.
100 N. A. Humaera, A. N. Fahri, B. Armynah and D. Tahir, *Luminescence*, 2021, **36**, 1354–1364, DOI: 10.1002/bio.4084.
101 M. A. Mousa, H. H. Abdelrahman, M. A. Fahmy, D. G. Ebrahim and A. H. E. Moustafa, *Sci. Rep.*, 2023, **13**, 1–9, DOI: 10.1038/s41598-023-39490-y.
102 K. G. Nguyen, M. Huš, I. A. Baragau, J. Bowen, T. Heil, A. Nicolaev, L. E. Abramiuc, A. Sapelkin, M. T. Sajjad and S. Kellici, *Small*, 2024, **20**, 2310587, DOI: 10.1002/smll.202310587.
103 R. Usha, R. Fairlin Jenitha and S. Sudhaparimala, *Indian J. Chem. Technol.*, 2022, **29**, 485–494, DOI: 10.56042/ijct.v29i5.61639.
104 W. Gao, S. Zhang, G. Wang, J. Cui, Y. Lu, X. Rong, Y. Luo, L. C. Zhang, Z. Cheng and C. Gao, *Anal. Chim. Acta*, 2023, **1277**, 341683, DOI: 10.1016/j.aca.2023.341683.
105 D. Yoo, Y. Park, B. Cheon and M. H. Park, *Nanoscale Res. Lett.*, 2019, **14**, 272, DOI: 10.1186/s11671-019-3088-6.
106 S. Jovanović, Z. Marković, M. Budimir, J. Prekodravac, D. Zmejkoski, D. Kepić, A. Bonasera and B. T. Marković, *Pharmaceutics*, 2023, **15**, 1170, DOI: 10.3390/pharmaceutics15041170.
107 D. Ozyurt, M. Al Kobaisi, R. K. Hocking and B. Fox, *Carbon Trends*, 2023, **12**, 100276, DOI: 10.1016/j.cartre.2023.100276.
108 S. A. Shaik, S. Sengupta, R. S. Varma, M. B. Gawande and A. Goswami, *ACS Sustainable Chem. Eng.*, 2021, **9**, 3–49, DOI: 10.1021/acssuschemeng.0c04727.
109 H. Barhum, T. Alon, M. Attrash, A. Machnev, I. Shishkin and P. Ginzburg, *ACS Appl. Nano Mater.*, 2021, **4**, 9919–9931, DOI: 10.1021/acsanm.1c02496.
110 L. Zhao, Y. Wang, X. Zhao, Y. Deng and Y. Xia, *Polymers*, 2019, **11**, 1731, DOI: 10.3390/polym11111731.
111 X. Luo, P. Bai, X. Wang, G. Zhao, J. Feng and H. Ren, *New J. Chem.*, 2019, **43**, 5488–5494, DOI: 10.1039/C8NJ06305B.
112 K. Chang, Q. Zhu, L. Qi, M. Guo, W. Gao and Q. Gao, *Materials*, 2022, **15**, 466, DOI: 10.3390/ma15020466.
113 X. Wu and H. Li, *Microchem. J.*, 2024, **201**, 110573, DOI: 10.1016/j.microc.2024.110573.
114 Z. Qian, J. Ma, X. Shan, H. Feng, L. Shao and J. Chen, *Chem. – Eur. J.*, 2014, **20**, 2254–2263, DOI: 10.1002/chem.201304374.
115 X. Dong, Y. Su, H. Geng, Z. Li, C. Yang, X. Li and Y. Zhang, *J. Mater. Chem. C*, 2014, **2**, 7477–7481, DOI: 10.1039/c4tc01139b.
116 M. Yang, Y. Yan, E. Liu, X. Hu, H. Hao and J. Fan, *Opt. Mater.*, 2021, **112**, 110743, DOI: 10.1016/j.optmat.2020.110743.
117 J. Gamboa, R. el Attar, D. Thuau, F. Estrany, M. Abbas and J. Torras, *Microchim. Acta*, 2024, **191**, 639, DOI: 10.1007/s00604-024-06722-5.
118 A. Hemmati, H. Emadi and S. R. Nabavi, *ACS Omega*, 2023, **8**, 20987–20999, DOI: 10.1021/acsomega.3c01795.
119 Z. Pu, Q. Wang, K. Li, W. Fan and M. Li, *Opt. Mater.*, 2023, **146**, 114598, DOI: 10.1016/j.optmat.2023.114598.
120 W. Liu, H. Jia, J. Zhang, J. Tang, J. Wang and D. Fang, *Microchem. J.*, 2020, **158**, 105187, DOI: 10.1016/j.microc.2020.105187.
121 C. Wang, H. Shi, M. Yang, Y. Yan, E. Liu, Z. Ji and J. Fan, *J. Photochem. Photobiol., A*, 2020, **391**, 112374, DOI: 10.1016/j.jphotochem.2020.112374.
122 B. W. An, Y. Q. Liu, C. Huang, Y. Wang, T. Zhu, J. G. Wang, Y. L. Leng, Y. P. Zhang, D. H. Zhang and X. H. Cai, *J. Colloid Interface Sci.*, 2026, **704**, 139380, DOI: 10.1016/j.jcis.2025.139380.
123 P. Li, F. Han, W. Cao, G. Zhang, J. Li, J. Zhou, X. Gong, G. Turnbull, W. Shu, L. Xia, B. Fang, X. Xing and B. Li, *Appl. Mater. Today*, 2020, **19**, 100601, DOI: 10.1016/j.apmt.2020.100601.
124 O. A. Aladesuyi and O. S. Oluwafemi, *Heliyon*, 2023, **9**, e15904, DOI: 10.1016/j.heliyon.2023.e15904.
125 B. S. Gómez Pineros and G. Granados-Oliveros, *J. Mol. Struct.*, 2024, **1317**, 138990, DOI: 10.1016/j.molstruc.2024.138990.
126 S. Chandra, P. Patra, S. H. Pathan, S. Roy, S. Mitra, A. Layek, R. Bhar, P. Pramanik and A. Goswami, *J. Mater. Chem. B*, 2013, **1**, 2375–2382, DOI: 10.1039/c3tb00583f.
127 F. Du, Z. Cheng, W. Tan, L. Sun and G. Ruan, *Spectrochim. Acta, Part A*, 2020, **226**, 117602, DOI: 10.1016/j.saa.2019.117602.
128 B. Dai, C. Wu, Y. Lu, D. Deng and S. Xu, *J. Lumin.*, 2017, **190**, 108–114, DOI: 10.1016/j.jlumin.2017.04.054.
129 S. Pei, Y. Wang, S. Cai, K. Yan, K. Luo and Y. Ma, *RSC Adv.*, 2025, **15**, 27294–27299, DOI: 10.1039/d5ra04505c.
130 D. Luo, H. Zhang, X. An, J. Zhao, C. Feng, J. Yin, M. Luo, T. Wei, Y. Liu, Y. Shi, J. Zhang and B. Lai, *J. Hazard. Mater.*, 2025, **494**, 138567, DOI: 10.1016/j.jhazmat.2025.138567.
131 F. Jia, H. Li, Z. Liu, Q. Gong, H. W. Luo, X. Ma, J. Hao and H. Pan, *Colloids Surf., A*, 2025, **725**, 137677, DOI: 10.1016/j.colsurfa.2025.137677.
132 S. R. Kamali, C. N. Chen, D. C. Agrawal and T. H. Wei, *J. Anal. Sci. Technol.*, 2021, **12**, 48, DOI: 10.1186/s40543-021-00298-y.
133 L. Zhang, Y. Wang, K. Wan, J. H. Piao and Z. X. Liang, *Electrochem. Commun.*, 2018, **86**, 53–56, DOI: 10.1016/j.elecom.2017.11.015.
134 F. Li, T. Li, C. Sun, J. Xia, Y. Jiao and H. Xu, *Angew. Chem., Int. Ed.*, 2017, **56**, 9910–9914, DOI: 10.1002/anie.201705989.
135 H. Su, Y. Lv, L. Zhu and Y. Wang, *Colloids Surf., B*, 2024, **234**, 113757, DOI: 10.1016/j.colsurfb.2024.113757.
136 K. Yin, B. Bao, J. Li, M. Wang, F. Wang, B. Sun, Y. Gong and F. Lian, *Chemosphere*, 2024, **364**, 143175, DOI: 10.1016/j.chemosphere.2024.143175.
137 W. Luo, Y. Wang, F. Lin, Y. Liu, G. Gu, W. Liu and C. Xiao, *Int. J. Nanomed.*, 2020, **15**, 10113–10125, DOI: 10.2147/IJN.S282985.
138 Z. T. Rosenkrans, T. Sun, D. Jiang, W. Chen, T. E. Barnhart, Z. Zhang, C. A. Ferreira, X. Wang, J. W. Engle, P. Huang

and W. Cai, *Adv. Sci.*, 2020, **7**, 2000420, DOI: 10.1002/advs.202000420.
139 J. Li, Z. Wang, Y. Zhang, X. Cao, F. Lian and S. Gu, *Environ. Sci.: Nano*, 2023, **10**, 866–878, DOI: 10.1039/d2en00918h.
140 D. Zhou, H. Huang, Y. Wang, J. Yu and Z. Hu, *IOP Conf. Ser.: Earth Environ. Sci.*, 2021, **692**, 032066, DOI: 10.1088/1755-1315/692/3/032066.
141 X. Shan, L. Chai, J. Ma, Z. Qian, J. Chen and H. Feng, *Analyst*, 2014, **139**, 2322–2325, DOI: 10.1039/c3an02222f.
142 X. Luo, Z. Wang, M. Yang, R. Lei, J. Yang, M. Li, H. Hao, Z. Liu, H. Tang, B. Peng, Y. Tian, K. Chen, Y. N. Chang, H. Yuan, J. Tong, L. Zhu, C. Lu, G. Xing and J. Li, *ACS Appl. Bio Mater.*, 2025, **8**, 5138–5146, DOI: 10.1021/acsabm.5c00479.
143 G. K. Güven, M. E. Okur, Ş. Ayla, G. Çalışkan, M. N. Al, L. Gülüm, Y. Tutar, N. Ü. Okur and İ. T. Değim, *Int. J. Pharm.*, 2025, **679**, 125745, DOI: 10.1016/j.ijpharm.2025.125745.
144 L. Yang, Q. Zhang, Y. Huang, C. Luo, Z. Quan, H. Li, S. Sun and Y. Xu, *J. Colloid Interface Sci.*, 2023, **632**, 129–139, DOI: 10.1016/j.jcis.2022.11.062.
145 M. A. A. Hamid, S. H. Elagamy, A. Gamal and F. R. Mansour, *J. Pharm. Biomed. Anal.*, 2024, **248**, 116270, DOI: 10.1016/j.jpba.2024.116270.
146 A. Truskewycz, B. Choi, L. Pedersen, J. Han, M. MacGregor and N. Halberg, *ACS Nano*, 2025, **19**, 33103–33117, DOI: 10.1021/acsnano.5c03108.
147 Q. Wang, J. Li, X. Tu, H. Liu, M. Shu, R. Si, C. T. J. Ferguson, K. A. I. Zhang and R. Li, *Chem. Mater.*, 2020, **32**, 734–743, DOI: 10.1021/acs.chemmater.9b03708.
148 Q. Fu, S. Sun, K. Lu, N. Li and Z. Dong, *Chin. Chem. Lett.*, 2024, **35**, 109136, DOI: 10.1016/j.cclet.2023.109136.
149 Q. Fu, S. Sun, N. Li, K. Lu and Z. Dong, *Mater. Today Chem.*, 2023, **34**, 101769, DOI: 10.1016/j.mtchem.2023.101769.
150 Y. Yu, Q. Zeng, S. Tao, C. Xia, C. Liu, P. Liu and B. Yang, *Adv. Sci.*, 2023, **10**, 2207621, DOI: 10.1002/advs.202207621.
151 G. Zuo, A. Xie, J. Li, T. Su, X. Pan and W. Dong, *J. Phys. Chem. C*, 2017, **121**, 26558–26565, DOI: 10.1021/acs.jpcc.7b10179.
152 G. Zuo, A. Xie, X. Pan, T. Su, J. Li and W. Dong, *ACS Appl. Nano Mater.*, 2018, **1**, 2376–2385, DOI: 10.1021/acsanm.8b00521.
153 T. Y. Luo, X. He, J. Zhang, P. Chen, Y. H. Liu, H. J. Wang and X. Q. Yu, *RSC Adv.*, 2018, **8**, 6053–6062, DOI: 10.1039/c7ra13607b.
154 J. Liu, X. Meng, Y. Song, Q. Jing and H. Zhao, *Surf. Interfaces*, 2025, **72**, 107102, DOI: 10.1016/j.surfin.2025.107102.
155 G. Murali, J. K. R. Modigunta, S. Park, S. Lee, H. Lee, J. Yeon, H. Kim, Y. H. Park, S. Y. Park, J. R. Durrant, H. Cha, T. K. An and I. In, *ACS Appl. Mater. Interfaces*, 2021, **13**, 34648–34657, DOI: 10.1021/acsami.1c01879.
156 S. Hu, Y. Ding, Q. Chang, J. Yang and K. Lin, *Appl. Surf. Sci.*, 2015, **355**, 774–777, DOI: 10.1016/j.apsusc.2015.07.125.
157 R. Knoblauch, A. Harvey, E. Ra, K. M. Greenberg, J. Lau, E. Hawkins and C. D. Geddes, *Nanoscale*, 2021, **13**, 85–99, DOI: 10.1039/d0nr06842j.
158 R. Knoblauch, B. Bui, A. Raza and C. D. Geddes, *Phys. Chem. Chem. Phys.*, 2018, **20**, 15518–15527, DOI: 10.1039/c8cp02675k.
159 K. Luo, W. Luo, Z. Liang, Y. Li, X. Kang, Y. Wu and Y. Wen, *New J. Chem.*, 2022, **46**, 19283–19290, DOI: 10.1039/d2nj03474c.
160 T. S. Atabaev, D. Askar, Z. Baranchiyeva, B. A. Zhainsabayeva, T. Elebessov, M. S. Kang, B. Duisenbayeva, E. A. Mun, T. T. Pham and D. W. Han, *Mater. Adv.*, 2024, **5**, 9000–9006, DOI: 10.1039/d4ma00823e.
161 P. Sidharthan, D. Senthilkumar, R. J. Chung, M. Govindasamy and C. Y. Kuo, *J. Taiwan Inst. Chem. Eng.*, 2025, 106456, DOI: 10.1016/j.jtice.2025.106456.
162 C. Shen, J. Wang, Y. Cao and Y. Lu, *J. Mater. Chem. C*, 2015, **3**, 6668–6675, DOI: 10.1039/c5tc01156f.
163 O. Ustun, S. N. Karadag, H. Mazlumoglu, A. Yilmaz and M. Yilmaz, *Coatings*, 2023, **13**, 456, DOI: 10.3390/coatings13020456.
164 Y. Wu, D. Qin, Z. Luo, S. Meng, G. Mo, X. Jiang and B. Deng, *ACS Sustainable Chem. Eng.*, 2022, **10**, 5195–5202, DOI: 10.1021/acssuschemeng.1c08676.
165 G. Magdy, N. Said, R. A. El-Domany and F. Belal, *BMC Chem.*, 2022, **16**, 98, DOI: 10.1186/s13065-022-00894-y.
166 G. Magdy, S. Ebrahim, F. Belal, R. A. El-Domany and A. M. Abdel-Megied, *Sci. Rep.*, 2023, **13**, 5502, DOI: 10.1038/s41598-023-32494-8.
167 M. Chaghaghazardi, S. Kashanian, M. Nazari, K. Omidfar, Y. Joseph and P. Rahimi, *Spectrochim. Acta, Part A*, 2023, **293**, 122448, DOI: 10.1016/j.saa.2023.122448.
168 H. Shi, Q. Zhao, C. Zhou and N. Jia, *Chin. J. Anal. Chem.*, 2022, **50**, 63–68, DOI: 10.1016/j.cjac.2021.09.010.
169 N. Ibrayev, R. Dzhanabekova, E. Seliverstova and G. Amanzholova, *Fullerenes, Nanotub. Carbon Nanostruct.*, 2022, **30**, 22–26, DOI: 10.1080/1536383X.2021.1999933.
170 X. Zhao, H. Wang, Q. Liu and X. Chen, *Talanta*, 2024, **269**, 125479, DOI: 10.1016/j.talanta.2023.125479.
171 O. A. Aladesuyi and O. S. Oluwafemi, *Inorg. Chem. Commun.*, 2023, **153**, 110843, DOI: 10.1016/j.inoche.2023.110843.
172 C. Wang, H. Shi, M. Yang, Z. Yao, B. Zhang, E. Liu, X. Hu, W. Xue and J. Fan, *Colloids Surf., B*, 2021, **205**, 111874, DOI: 10.1016/j.colsurfb.2021.111874.
173 G. Huang, Y. Lin, L. Zhang, Z. Yan, Y. Wang and Y. Liu, *Sci. Rep.*, 2019, **9**, 19651, DOI: 10.1038/s41598-019-55996-w.
174 A. Priyadharshini and A. A. Napoleon, *Inorg. Chem. Commun.*, 2025, **179**, 114716, DOI: 10.1016/j.inoche.2025.114716.
175 A. M. A. Saputra, A. F. R. Piliang, Dellyansyah, Marpongahtun, Andriayani, R. Goei, R. R. Risky and S. Gea, *Catal. Commun.*, 2024, **187**, 106914, DOI: 10.1016/j.catcom.2024.106914.
176 M. R. Malini, B. K. Devendra, H. R. Panchami, N. Kottam and B. S. Krishna, *Synth. Met.*, 2026, **316**, 117977, DOI: 10.1016/j.synthmet.2025.117977.
177 D. Cai, X. Zhong, L. Xu, Y. Xiong, W. Deng, G. Zou, H. Hou and X. Ji, *Chem. Sci.*, 2025, **16**, 4937–4970, DOI: 10.1039/d4sc08659g.
178 M. Liu, Y. Xu, F. Niu, J. J. Gooding and J. Liu, *Analyst*, 2016, **141**, 2657–2664, DOI: 10.1039/c5an02231b.

179 L. Chen, J. Wei, C. Zhang, Z. Du, H. Li and W. Zou, *RSC Adv.*, 2014, **4**, 51084–51088, DOI: 10.1039/c4ra07292h.
180 H. M. Solayman, K. H. Leong, M. K. Hossain, M. B. Khan, K. Kang, J. J. Jiang and A. Abd Aziz, *Next Mater.*, 2025, **8**, 100787, DOI: 10.1016/j.nxmate.2025.100787.
181 W. Tan, G. Yao, H. Yu, Y. He, M. Lu, T. Zou, X. Li, P. Yin, P. Na, W. Yang, M. Yang and H. Wang, *Food Chem.*, 2024, **447**, 139020, DOI: 10.1016/j.foodchem.2024.139020.
182 J. Wang, Y. X. Zhu, X. F. Xie, X. He, J. T. Fan and A. Y. Chen, *J. Environ. Chem. Eng.*, 2022, **10**, 107112, DOI: 10.1016/j.jece.2021.107112.
183 L. Cui, X. Ren, M. Sun, H. Liu and L. Xia, *Nanomaterials*, 2021, **11**, 3419, DOI: 10.3390/nano11123419.
184 P. D. Modi, V. N. Mehta, V. S. Prajapati, S. Patel and J. V. Rohit, *Carbon Dots Anal. Chem. Detect. Imaging*, 2022, pp. 15–29, DOI: 10.1016/B978-0-323-98350-1.00022-0.
185 V. Agarwal, A. Chakraborty, A. Prasun, T. K. Sahu and T. K. Sarma, *ChemCatChem*, 2025, **17**, e00414, DOI: 10.1002/cctc.202500414.
186 N. Ullal, R. Mehta and D. Sunil, *Analyst*, 2024, **149**, 1680–1700, DOI: 10.1039/d3an02134c.
187 H. L. Yang, L. F. Bai, Z. R. Geng, H. Chen, L. T. Xu, Y. C. Xie, D. J. Wang, H. W. Gu and X. M. Wang, *Mater. Today Adv.*, 2023, **18**, 100376, DOI: 10.1016/j.mtadv.2023.100376.
188 S. Kumar, J. Gaur, S. Kaushal, J. Dalal, M. Misra, H. Kaur, S. Kaur, N. Kaur, G. Singh and G. Singh, *Crystals*, 2025, **15**, 320, DOI: 10.3390/cryst15040320.
189 H. L. Yang, M. B. M. Y. Ang, H. A. Tsai, K. R. Lee and J. Y. Lai, *J. Taiwan Inst. Chem. Eng.*, 2022, **133**, 104250, DOI: 10.1016/j.jtice.2022.104250.
190 B. K. Barman, Ø. Sele Handegård, A. Hashimoto and T. Nagao, *ACS Sustainable Chem. Eng.*, 2021, **9**, 9879–9890, DOI: 10.1021/acssuschemeng.1c02791.
191 A. G. El-Shamy and H. S. S. Zayied, *Synth. Met.*, 2020, **259**, 116218, DOI: 10.1016/j.synthmet.2019.116218.
192 Z. Latif, H. B. Albargi, Z. Khaliq, K. Shahid, U. Khalid, M. B. Qadir, M. Ali, S. N. Arshad, A. S. Alkorbi, M. Jalalah and M. Jalalah, *Nanoscale Adv*, 2024, **6**, 1750–1764, DOI: 10.1039/d3na01143g.
193 R. Guo, X. Yuan, X. Zhou, H. Chen, H. Xie, Q. Hu, H. Luo and D. Zhang, *Polymers*, 2025, **17**, 390, DOI: 10.3390/polym17030390.
194 X. Jian, H. Min Yang, J. Gang Li, E. Hui Zhang, L. Le Cao and Z. Hai Liang, *Electrochim. Acta*, 2017, **228**, 483–493, DOI: 10.1016/j.electacta.2017.01.082.
195 L. Li, Y. Wang, Z. Gao, X. Mao, X. Zhang, W. Xing, C. Jia, L. Huang and J. Tang, *Dyes Pigm.*, 2024, **224**, 111977, DOI: 10.1016/j.dyepig.2024.111977.
196 F. Mohtaram, M. Petersen, M. Ahrenst-Mortensen, L. S. Boysen, F. H. Gram, H. H. Malling, N. F. H. Bang, Y. J. Hess and P. Fojan, *Materials*, 2024, **17**, 6242, DOI: 10.3390/ma17246242.
197 W. Qin, L. Zou, Y. Hou, Z. Wu, D. A. Loy and D. Lin, *Chem. Eng. J.*, 2024, **496**, 154041, DOI: 10.1016/j.cej.2024.154041.
198 A. Partovi, M. Khedrinia, S. Arjmand and S. O. Ranaei Siadat, *Sci. Rep.*, 2024, **14**, 19256, DOI: 10.1038/s41598-024-70295-9.
199 W. Song, X. Zhai, J. Shi, X. Zou, Y. Xue, Y. Sun, W. Sun, J. Zhang, X. Huang, Z. Li, T. Shen, Y. Li, C. Zhou, M. Holmes, Y. Gong and M. Povey, *Food Chem.*, 2024, **434**, 137423, DOI: 10.1016/j.foodchem.2023.137423.
200 L. Sai, K. Ke, Y. Cai, S. Dong, H. Jia, L. Cao, Z. Wu and F. Wang, *Appl. Mater. Today*, 2024, **36**, 102025, DOI: 10.1016/j.apmt.2023.102025.
201 X. Nie, S. Wu, A. Mensah, K. Lu and Q. Wei, *Mater. Sci. Eng. C*, 2020, **108**, 110377, DOI: 10.1016/j.msec.2019.110377.
202 H. W. Chen, Y. L. Kuo, S. H. Huang, C. S. Chiou, Y. C. Chen and W. T. Chen, *J. Environ. Chem. Eng.*, 2024, **12**, 111680, DOI: 10.1016/j.jece.2023.111680.
203 Y. L. Kuo, W. T. Chen, C. H. Chen, H. T. Wu, C. S. Chiou, Y. C. Chen and H. W. Chen, *Mater. Chem. Phys.*, 2024, **316**, 129079, DOI: 10.1016/j.matchemphys.2024.129079.
204 G. Viscusi, S. Mottola, H. A. S. Tohamy, G. Gorrasi and I. De Marco, *Lect. Notes Civ. Eng.*, 2024, **525**, 133–137, DOI: 10.1007/978-3-031-63357-7_22.
205 A. Jayakumar, S. Radoor, G. H. Shin and J. T. Kim, *Ind. Crops Prod.*, 2024, **209**, 117968, DOI: 10.1016/j.indcrop.2023.117968.
206 J. R. Ansari, K. Park and J. Seo, *Food Packag. Shelf Life*, 2025, **48**, 101460, DOI: 10.1016/j.fpsl.2025.101460.
207 X. Tao, M. Liao, F. Wu, Y. Jiang, J. Sun and S. Shi, *Chem. Eng. J.*, 2022, **443**, 136442, DOI: 10.1016/j.cej.2022.136442.
208 L. Xu, Y. Zhang, H. Pan, N. Xu, C. Mei, H. Mao, W. Zhang, J. Cai and C. Xu, *Materials*, 2020, **13**, 67, DOI: 10.3390/ma13010067.
209 L. Wang, X. Liu, P. Qi, J. Sun, S. Jiang, H. Li, X. Gu and S. Zhang, *Carbohydr. Polym.*, 2022, **278**, 118957, DOI: 10.1016/j.carbpol.2021.118957.
210 E. Jamróz, P. Kopel, J. Tkaczewska, D. Dordevic, S. Jancikova, P. Kulawik, V. Milosavljevic, K. Dolezelikova, K. Smerkova, P. Svec and V. Adam, *Polymers*, 2019, **11**, 2046, DOI: 10.3390/polym11122046.
211 A. Boruah, S. Bora, A. Thakur, H. S. Dutta and B. K. Saikia, *ACS Omega*, 2023, **8**(28), 25410–25423, DOI: 10.1021/acsomega.3c02884.
212 E. Colusso, L. Cicerchia, M. Rigon, V. Gomes and A. Martucci, *J. Sol-Gel Sci. Technol.*, 2023, **107**, 170–177, DOI: 10.1007/s10971-022-05742-y.
213 K. Liu, F. Liu and Y. Xu, *Microchim. Acta*, 2025, **192**, 91, DOI: 10.1007/s00604-024-06937-6.
214 M. J. Khan, Z. Karim, P. Pongchaikul, P. Posoknistakul, P. Intra, N. Laosiripojana, K. C. W. Wu and C. Sakdaronnarong, *J. Taiwan Inst. Chem. Eng.*, 2024, **160**, 105324, DOI: 10.1016/j.jtice.2023.105324.
215 J. Wu, Q. Lu, H. Wang and B. Huang, *Nanomaterials*, 2022, **12**, 2624, DOI: 10.3390/nano12152624.
216 Z. Tian, S. Qin, J. Yang, X. Wu, J. Zhang, J. Li, H. Wang and Z. Cui, *Appl. Surf. Sci.*, 2024, **661**, 160078, DOI: 10.1016/j.apsusc.2024.160078.
217 S. Kalytchuk, Y. Wang, K. Poláková and R. Zbořil, *ACS Appl. Mater. Interfaces*, 2018, **10**(35), 29902–29908, DOI: 10.1021/acsami.8b11663.
218 N. K. Stanković, B. M. T. Marković and Z. M. Marković, *J. Serbian Chem. Soc.*, 2020, **85**, 1095–1127, DOI: 10.2298/JSC191225008S.

219 M. Bodik, P. Siffalovic, P. Nadazdy, M. Benkovicova, Z. Markovic, J. Chlpik, J. Cirak, M. Kotlar, M. Micusik, M. Jergel and E. Majkova, *Diamond Relat. Mater.*, 2018, **83**, 170–176, DOI: 10.1016/j.diamond.2018.02.011.

220 N. K. Stanković, M. Bodik, P. Šiffalovič, M. Kotlar, M. Mičušik, Z. Špitalsky, M. Danko, D. D. Milivojević, A. Kleinova, P. Kubat, Z. Capakova, P. Humpoliček, M. Lehocky, B. M. Todorović Marković and Z. M. Marković, *ACS Sustainable Chem. Eng.*, 2018, **6**(3), 4154–4163, DOI: 10.1021/acssuschemeng.7b04566.

221 T. Vyas, H. Kumar, S. Choudhary and A. Joshi, *Environ. Sci. Water Res. Technol.*, 2024, **10**, 2858–2868, DOI: 10.1039/d4ew00452c.

222 T. Vyas and A. Joshi, *Analyst*, 2024, **149**, 1297–1309, DOI: 10.1039/d3an01571h.

223 Y. Li, H. Zhou, Q. Jiang, S. Zheng, Y. Wei and Q. Zhang, *J. Electrochem. Soc.*, 2024, **171**, 037501, DOI: 10.1149/1945-7111/ad2cc3.

224 T. Vyas and A. Joshi, *Opt. Mater.*, 2024, **154**, 115700, DOI: 10.1016/j.optmat.2024.115700.

225 T. Vyas, M. A. Sadique, J. Lodhi, A. Joshi and R. Khan, *ACS Appl. Nano Mater.*, 2025, **8**(23), 11811–11822, DOI: 10.1021/acsanm.5c00872.

226 Q. Huang, S. Hu, H. Zhang, J. Chen, Y. He, F. Li, W. Weng, J. Ni, X. Bao and Y. Lin, *Analyst*, 2013, **138**, 5417–5423, DOI: 10.1039/c3an00510k.

227 T. Vyas, S. Jaiswal, S. Choudhary, P. Kodgire and A. Joshi, *Environ. Res.*, 2024, **243**, 117855, DOI: 10.1016/j.envres.2023.117855.

228 W. A. Amer, M. E. Abdelghafar, J. Stejskal and M. M. Ayad, *Mater. Sci. Eng., Part B*, 2025, **322**, 118612, DOI: 10.1016/j.mseb.2025.118612.

229 H. Ren, Q. Li, L. Han, X. Liu, X. Huang, Z. Pang and J. Zhang, *Int. J. Biol. Macromol.*, 2025, **309**, 142922, DOI: 10.1016/j.ijbiomac.2025.142922.

230 Y. Zhao, M. Li, N. Zhou, S. Xu, M. Shi, C. Huang and H. Mao, *Sens. Actuators, B*, 2024, **407**, 135493, DOI: 10.1016/j.snb.2024.135493.

231 J. Liu, H. Yu, S. Yang, F. Feng, H. Meng, X. Zhang and Y. Gao, *Opt. Commun.*, 2025, **574**, 131061, DOI: 10.1016/j.optcom.2024.131061.

232 J. Sun, K. Yan, P. Zhang, A. Pan, W. Xiong, X. Chen, C. Zhao and J. Hong, *Colloids Surf., A*, 2024, **695**, 134286, DOI: 10.1016/j.colsurfa.2024.134286.

233 L. E. da Silva, O. L. de, L. Calado, S. F. de Oliveira Silva, K. R. M. da Silva, J. Henrique Almeida, M. de Oliveira Silva, R. da, S. Viana, J. N. de Souza Ferro, J. de Almeida Xavier and C. D. A. E. S. Barbosa, *J. Colloid Interface Sci.*, 2023, **651**, 678–685, DOI: 10.1016/j.jcis.2023.07.124.

234 J. Sun, K. Yan, P. Zhang, A. Pan, X. Chen and X. Shi, *Lubricants*, 2024, **12**, 88, DOI: 10.3390/lubricants12030088.

235 M. J. Molaei, *RSC Adv.*, 2019, **9**, 6460–6481, DOI: 10.1039/c8ra08088g.

236 Y. Xiao, Z. Wang, J. Fu, J. Zhang, Q. He, H. Lu, Q. Zhou and H. Wang, *Water*, 2025, **17**, 210, DOI: 10.3390/w17020210.

237 Y. F. Mi, Y. H. Huang, S. H. He, R. Ma, Y. D. Meng and Z. H. Cao, *Sep. Purif. Technol.*, 2023, **317**, 123870, DOI: 10.1016/j.seppur.2023.123870.

238 D. L. Zhao and T. S. Chung, *Water Res.*, 2018, **147**, 43–49, DOI: 10.1016/j.watres.2018.09.040.

239 C. X. Guo, D. Zhao, Q. Zhao, P. Wang and X. Lu, *Chem. Commun.*, 2014, **50**, 7318–7321, DOI: 10.1039/c4cc01603c.

240 W. Gai, D. L. Zhao and T. S. Chung, *Water Res.*, 2019, **154**, 54–61, DOI: 10.1016/j.watres.2019.01.043.

241 H. Sun and P. Wu, *J. Membr. Sci.*, 2018, **564**, 394–403, DOI: 10.1016/j.memsci.2018.07.044.

242 Z. Yuan, X. Wu, Y. Jiang, Y. Li, J. Huang, L. Hao, J. Zhang and J. Wang, *J. Membr. Sci.*, 2018, **549**, 1–11, DOI: 10.1016/j.memsci.2017.11.051.

243 H. L. Yang, C. T. Huang, H. Y. Lin, Y. H. Chen, H. A. Tsai and K. R. Lee, *Sep. Purif. Technol.*, 2024, **331**, 125709, DOI: 10.1016/j.seppur.2023.125709.

244 K. Shen, G. Luo, J. Liu, J. Zheng and C. Xu, *Sol. Energy Mater. Sol. Cells*, 2019, **193**, 372–378, DOI: 10.1016/j.solmat.2019.01.004.

245 M. Pourmadadi, E. Rahmani, M. Rajabzadeh-Khosroshahi, A. Samadi, R. Behzadmehr, A. Rahdar and L. F. R. Ferreira, *J. Drug Deliv. Sci. Technol.*, 2023, **80**, 104156, DOI: 10.1016/j.jddst.2023.104156.

246 T. Qin, L. Deng, J. Zhang, N. Zhang, P. Zhang, Y. Liu, L. Qin, S. Huang, L. Qiu and S. Peng, *Ceram. Int.*, 2024, **50**, 53254–53263, DOI: 10.1016/j.ceramint.2024.10.175.

247 R. Bandi, N. P. Devulapalli, R. Dadigala, B. R. Gangapuram and V. Guttena, *ACS Omega*, 2018, **3**(10), 13454–13466, DOI: 10.1021/acsomega.8b01743.

248 L. Thyda, J. K. Joseph, K. Naresh, G. Dasi, S. Suneetha, R. Thangavel, V. Jayalakshmi, P. Amaladass and K. Thangaraju, *Appl. Surf. Sci.*, 2025, **685**, 162032, DOI: 10.1016/j.apsusc.2024.162032.

249 L. Thyda, K. Naresh, J. K. Joseph, S. Suneetha, C. E. Jeyanthi, P. Amaladass, C. Selvaraju and K. Thangaraju, *Thin Solid Films*, 2024, **790**, 140221, DOI: 10.1016/j.tsf.2024.140221.

250 C. Yao, Q. Wu and T. Tian, *Ceram. Int.*, 2024, **50**, 51832–51840, DOI: 10.1016/j.ceramint.2024.02.217.

251 G. Yang, X. Wan, Y. Liu, R. Li, Y. Su, X. Zeng and J. Tang, *ACS Appl. Mater. Interfaces*, 2016, **8**(50), 34744–34754, DOI: 10.1021/acsami.6b11476.

252 R. Kumar, B. Ranjan, K. Kumar, S. Shankhdhar and D. Kaur, *ACS Appl. Nano Mater.*, 2024, **7**(7), 7663–7673, DOI: 10.1021/acsanm.4c00366.

253 M. R. Pallavolu, S. Prabhu, R. R. Nallapureddy, A. S. Kumar, A. N. Banerjee and S. W. Joo, *Carbon*, 2023, **202**, 93–102, DOI: 10.1016/j.carbon.2022.10.077.

254 E. Dhandapani, N. Duraisamy and R. Rajedran, *ACS Appl. Polym. Mater.*, 2023, **5**(9), 7420–7432, DOI: 10.1021/acsapm.3c01237.

255 S. Ren, B. Liu, M. Wang, G. Han, H. Zhao and Y. Zhang, *J. Mater. Chem. C*, 2022, **10**, 11338–11346, DOI: 10.1039/d2tc02664c.

256 W. Luo, H. Quan, Z. Zhang, Y. Wang, X. Xie, Z. Hong and D. Chen, *ACS Appl. Nano Mater*, 2021, **4**, 12051–12061, DOI: 10.1021/acsanm.1c02606.

257 D. Sujatha, P. Nandigana, P. Sriram and S. K. Panda, *Carbon Quantum Dots Sustainable Energy Optoelectron.*, 2023, pp. 55–90, DOI: 10.1016/B978-0-323-90895-5.00007-2.
258 A. A. Maxim, S. N. Sadyk, D. Aidarkhanov, C. Surya, A. Ng, Y. H. Hwang, T. S. Atabaev and A. N. Jumabekov, *Nanomaterials*, 2020, **10**, 291, DOI: 10.3390/nano10020291.
259 W. Liu, Z. Ma, X. Jin, L. Lin, J. Zheng and W. Lau, *Prog. Photovoltaics Res. Appl.*, 2025, **33**, 1056–1067, DOI: 10.1002/pip.3917.
260 W. Li, Y. Han, L. Wang, G. S. Selopal, X. Wang and H. Zhao, *RSC Adv.*, 2024, **14**, 83–89, DOI: 10.1039/d3ra07235e.
261 X. Guo, R. Yang, Y. Wang, C. Cheng, D. Fu and J. Sheng, *Int. J. Biol. Macromol.*, 2023, **253**, 126723, DOI: 10.1016/j.ijbiomac.2023.126723.
262 M. Aksu and Ö. Güzdemir, *Food Bioprocess Technol.*, 2025, **18**, 6753–6778, DOI: 10.1007/s11947-025-03854-1.
263 V. Manikandan and S. C. Min, *Food Sci. Biotechnol.*, 2023, **32**, 1159–1171, DOI: 10.1007/s10068-023-01309-x.
264 D. Gupta, R. Priyadarshi, S. K. Tammina, J. W. Rhim and G. Agrawal, *Food Bioprocess Technol.*, 2025, **18**, 2145–2169, DOI: 10.1007/s11947-024-03578-8.
265 L. Deepika, Kumar and K. K. Gaikwad, *Sustainable Food Technol.*, 2023, **1**, 185–199, DOI: 10.1039/d2fb00020b.
266 G. Na and J. W. Kang, *Food Hydrocolloids*, 2025, **168**, 111568, DOI: 10.1016/j.foodhyd.2025.111568.
267 G. Bijoy and D. Sangeetha, *J. Environ. Chem. Eng.*, 2024, **12**, 113727, DOI: 10.1016/j.jece.2024.113727.
268 W. Li, X. Jin, X. Ma, B. Huang, X. Zhang, X. Li, Q. Si and W. Chen, *Mater. Sci. Eng., B*, 2025, **313**, 117978, DOI: 10.1016/j.mseb.2025.117978.
269 S. W. Park, S. H. Im, W. T. Hong, H. K. Yang and Y. K. Jung, *Int. J. Biol. Macromol.*, 2024, **268**, 131919, DOI: 10.1016/j.ijbiomac.2024.131919.
270 N. Rezvan and H. Shekarchizadeh, *J. Food Meas. Charact.*, 2024, **18**, 676–687, DOI: 10.1007/s11694-023-02197-9.
271 L. S. Ahmadi and A. R. Bahramian, *J. Dispers. Sci. Technol.*, 2025, 1–10, DOI: 10.1080/01932691.2025.2456988.
272 Z. Riahi, J. W. Rhim, R. Bagheri, G. Pircheraghi and E. Lotfali, *Prog. Org. Coatings*, 2022, **166**, 106794, DOI: 10.1016/j.porgcoat.2022.106794.
273 J. Zhang, J. Zhang, X. Huang, X. Zhai, Z. Li, J. Shi, R. Sobhy, I. Khalifa and X. Zou, *Food Res. Int.*, 2025, **202**, 115736, DOI: 10.1016/j.foodres.2025.115736.
274 S. Zhu, L. Jin, Y. Zhang, F. Chen, A. Farouk, T. Yang, G. Yi, H. Li, Z. J. Ban and L. Liu, *Sci. Rep.*, 2025, **15**, 25108, DOI: 10.1038/s41598-025-07882-x.
275 P. Ezati, J. W. Rhim, R. Molaei and Z. Rezaei, *Food Packag. Shelf Life*, 2022, **33**, 100878, DOI: 10.1016/j.fpsl.2022.100878.
276 P. Ezati and J. W. Rhim, *Colloids Surf., B*, 2022, **219**, 112804, DOI: 10.1016/j.colsurfb.2022.112804.
277 F. Wen, P. Li, H. Yan and W. Su, *Carbohydr. Polym.*, 2023, **311**, 120784, DOI: 10.1016/j.carbpol.2023.120784.
278 P. Das, S. Ganguly, S. R. Ahmed, M. Sherazee, S. Margel, A. Gedanken, S. Srinivasan and A. R. Rajabzadeh, *ACS Appl. Polym. Mater.*, 2022, **4**, 9323–9340, DOI: 10.1021/acsapm.2c01579.
279 B. D. Mansuriya and Z. Altintas, *Nanomaterials*, 2021, **11**, 2525, DOI: 10.3390/nano11102525.
280 S. J. Hong, S. Y. Ha, G. H. Shin and J. T. Kim, *Int. J. Biol. Macromol.*, 2024, **267**, 131397, DOI: 10.1016/j.ijbiomac.2024.131397.
281 M. Abbaszadeh, N. Arsalani, F. Kazeminava and A. Mahoutforoush, *Carbohydr. Polym. Technol. Appl.*, 2025, **11**, 100906, DOI: 10.1016/j.carpta.2025.100906.
282 F. Wen, W. Su, L. Cen, Y. Chen, L. Huo, H. Zhong and P. Li, *Int. J. Biol. Macromol.*, 2025, **306**, 141716, DOI: 10.1016/j.ijbiomac.2025.141716.
283 M. Wang, Y. Su, Y. Liu, Y. Liang, S. Wu, N. Zhou and J. Shen, *J. Colloid Interface Sci.*, 2022, **608**, 973–983, DOI: 10.1016/j.jcis.2021.10.018.
284 X. Dong, W. Liang, M. J. Meziani, Y. P. Sun and L. Yang, *Theranostics*, 2020, **10**, 671–686, DOI: 10.7150/thno.39863.
285 F. Kazeminava, S. Javanbakht, M. Nouri, P. Gholizadeh, P. Nezhad-Mokhtari, K. Ganbarov, A. Tanomand and H. S. Kafil, *J. Biol. Eng.*, 2022, **16**, 36, DOI: 10.1186/s13036-022-00318-4.
286 Z. M. Marković, M. D. Budimir, M. Danko, D. D. Milivojević, P. Kubat, D. Z. Zmejkoski, V. B. Pavlović, M. M. Mojsin, M. J. Stevanović and B. M. T. Marković, *Beilstein J. Nanotechnol.*, 2023, **14**, 165–174, DOI: 10.3762/bjnano.14.17.
287 A. Gaikwad, M. Joshi, K. Patil, S. Sathaye and C. Rode, *ACS Appl. Bio Mater.*, 2019, **2**, 5829–5840, DOI: 10.1021/acsabm.9b00795.
288 J. R. Ansari, K. Park, K. Sadeghi and J. Seo, *Food Packag. Shelf Life*, 2025, **49**, 101504, DOI: 10.1016/j.fpsl.2025.101504.
289 C. S. Fathima, A. M. Murali, S. K. Sachith and S. Daniel, *J. Food Eng.*, 2025, **397**, 112575, DOI: 10.1016/j.jfoodeng.2025.112575.
290 H. Du, L. He, J. Zhang and H. X. Lu, *LWT*, 2024, **208**, 116746, DOI: 10.1016/j.lwt.2024.116746.
291 S. J. Park, J. Y. Park, J. W. Chung, H. K. Yang, B. K. Moon and S. S. Yi, *Chem. Eng. J.*, 2020, **383**, 123200, DOI: 10.1016/j.cej.2019.123200.
292 Z. Yu, L. Zhang, X. Wang, D. He, H. Su and C. Zhao, *Sensors*, 2020, **20**, 4961, DOI: 10.3390/s20174961.
293 E. Dhandapani, P. Sengodan, N. Duraisamy and R. Ramesh, *Int. J. Energy Res.*, 2022, **46**, 7277–7292, DOI: 10.1002/er.7636.
294 Y. Liu, X. Wang, X. Shi and S. Wu, *Small*, 2026, e14630, DOI: 10.1002/smll.202514630.
295 Z. Ma, B. Zhang, H. Chen, F. Yue, L. Cheng, W.-M. Lau and D. Zhou, *Chem. Eng. J.*, 2026, **529**, 173206, DOI: 10.1016/j.cej.2026.173206.
296 T. Patel, S. Balu, D. Ganapathy and A. K. Sundramoorthy, *Anal. Methods*, 2026, **18**, 423–437, DOI: 10.1039/d5ay01457c.
297 Z. R. Ajahar Khan and J.-W. R. Jun Tae Kim, *Int. J. Biol. Macromol.*, 2026, **350**, 150956, DOI: 10.1016/j.ijbiomac.2026.150956.
298 D. Fang, B. Deng, C. Shi, Y. Wang, Z. Huang, L. Lyu, Y. Wu, F. Cao and W. Li, *Food Packag. Shelf Life*, 2026, **54**, 101724, DOI: 10.1016/j.fpsl.2026.101724.

299 D. Fang, B. Deng, C. Shi, Y. Wang, Z. Huang, L. Lyu, Y. Wu, F. Cao and W. Li, *Food Packag. Shelf Life*, 2026, **54**, 101724, DOI: 10.1016/j.fpsl.2026.101724.
300 N. Nammahachak, K. K. Aup-Ngoen, P. Asanithi, M. Horpratum, S. Chuangchote, S. Ratanaphan and W. Surareungchai, *RSC Adv.*, 2022, **12**, 31729–31733, DOI: 10.1039/d2ra05989d.
301 M. R. Hasan, N. Saha, T. Quaid and M. Toufiq Reza, *Energies*, 2021, **14**, 986, DOI: 10.3390/en14040986.
302 Q. B. Hoang, V. T. Mai, D. K. Nguyen, D. Q. Truong and X. D. Mai, *Mater. Today Chem.*, 2019, **12**, 166–172, DOI: 10.1016/j.mtchem.2019.01.003.
303 H. H. Jing, M. Adnan, M. Patel and S. Sasidharan, *Microchim. Acta*, 2025, **192**, 835, DOI: 10.1007/s00604-025-07683-z.
304 M. Vargas-Reyes, N. Bruna, J. Ramos-Zúñiga, F. Valenzuela-Ibaceta, P. Rivas-Álvarez, C. A. Navarro and J. M. Pérez-Donoso, *Microb. Cell Fact.*, 2024, **23**, 140, DOI: 10.1186/s12934-024-02417-x.
305 X. Kou, S. Jiang, S. J. Park and L. Y. Meng, *Dalton Trans.*, 2020, **49**, 6915–6938, DOI: 10.1039/d0dt01004a.
306 S. Dua, P. Kumar, B. Pani, A. Kaur, M. Khanna and G. Bhatt, *RSC Adv.*, 2023, **13**, 13534–13547, DOI: 10.1039/D3RA01556D.
307 T. Ahmed, H. Kuo and D. Lien, *Adv. Photonics Res.*, 2024, **5**, 2300216, DOI: 10.1002/adpr.202300216.
308 M. Havrdova, K. Hola, J. Skopalik, K. Tomankova, M. Petr, K. Cepe, K. Polakova, J. Tucek, A. B. Bourlinos and R. Zboril, *Carbon*, 2016, **99**, 238–248, DOI: 10.1016/j.carbon.2015.12.027.
309 T. Wu, K. Liu, S. Chen, Z. Ye, X. Xia, J. He, P. Xing, J. Yang, Y. Qian and M. Chen, *J. Hazard. Mater.*, 2025, **487**, 137255, DOI: 10.1016/j.jhazmat.2025.137255.
310 R. Khan, S. Shukla, M. Kumar, D. Barceló, A. Zuorro and P. C. Bhargava, *Environ. Res.*, 2024, **261**, 119671, DOI: 10.1016/j.envres.2024.119671.
311 K. Sharma, A. Singh, R. Roopashree, J. Sharma, J. Gaur, S. Kumar and S. Kaushal, *ChemistrySelect*, 2025, **10**, e00774, DOI: 10.1002/slct.202500774.
312 V. Manikandan and N. Y. Lee, *Environ. Res.*, 2022, **212**, 113280, DOI: 10.1016/j.envres.2022.113280.
313 J. Strickland, E. Haugabrooks, D. G. Allen, L. B. Balottin, Y. Hirabayashi, N. C. Kleinstreuer, H. Kojima, C. Nishizawa, P. Prieto, D. E. Ratzlaff, J. Jeong, J. H. Lee, Y. Yang, P. Lin, K. Sullivan and W. Casey, *Crit. Rev. Toxicol.*, 2023, **53**, 385–411, DOI: 10.1080/10408444.2023.2240852.
314 F. D. Rodríguez-Gómez, D. Monferrer, O. Penon and P. Rivera-Gil, *Front. Med.*, 2025, **12**, 1544393, DOI: 10.3389/fmed.2025.1544393.
315 B. Rooj and U. Mandal, *Vietnam J. Chem.*, 2023, **61**, 693–718, DOI: 10.1002/vjch.202300022.